

PART I: DESIGN AND SYNTHESIS OF ORGANIC MATERIALS FOR DYE SENSITIZED  
SOLAR CELLS  
PART II: QUALITATIVE AND SEMI-QUANTITATIVE STUDY OF THE BEHAVIOR OF  
SURFACTANT ON CRUDE OIL RECOVERY PROCESSES

Gayani Wasana Premathilake Pinnawala Arachchilage

A Thesis

Submitted to the Graduate College of Bowling Green  
State University in partial fulfillment of  
the requirements for the degree of

MASTER OF SCIENCE

August 2010

Committee:

Thomas Kinstle, Advisor

John Cable

Alexander Tarnovsky

Upali Weerasooriya

© 2010

Gayani Pinnawala Arachchilage

All Rights Reserved

## ABSTRACT

Thomas Kinstle, Advisor

The design and synthesis of new  $\pi$ -conjugated organic materials are currently at the forefront of research in order to realize stable and efficient organic electronic devices. Linear hydrocarbons and carbazole based materials are examples of  $\pi$ -conjugated organic systems widely studied for electronic applications.

Structural modifications increase the stability, improve the solubility, and improve the thin film packing and mobility compared to the parent substances. The electronic, physical, and photophysical properties of carbazole based materials in particular, can be easily modified by changing the substitution pattern on the main carbon skeleton.

Carbazole containing compound **1** shows an absorption maxima at 425 nm in dichloromethane and it is weakly soluble in other common organic solvents. This compound shows very weak emission.

An alcohol dimerization process known as the Guerbet reaction is used to create large alcohol structures for the production of the corresponding alkoxy sulfate surfactants. In the alcohol industry, Guerbet (dimer) alcohols are considered the “gold” standard for large, branched alcohols. These Guerbet alcohols tend to be more expensive than other alcohols when produced in high purity for various industrial applications. The high cost is mainly due to driving the reaction to completion and/or removing the unreacted monomer alcohol to produce high purity product. However, inexpensive Guerbet alcohols (GA) can be prepared by aiming for less than quantitative conversion during the alcohol dimerization process. The

resultant blend of 85-95% GA and 5-15% monomer alcohol is subsequently used in the alkoxylation process to add propylene oxide and/or ethylene oxide, followed by sulfation. Obtaining both ultra-low interfacial tension and low microemulsion viscosity when the equivalent alkane carbon number of the crude oil is high requires surfactants with very large hydrophobes and branched structures. Through the use of this new Guerbet process, these surfactants can be manufactured at low cost when made as sulfates as opposed to sulfonates. For example, a C32 GA can be produced from a C16 alcohol. This is a breakthrough in lowering the cost of surfactant flooding in high-temperature, high-salinity oil reservoirs because such surfactants are very salinity and temperature tolerant and cost much less than alkoxy sulfonates. Numerous microemulsion phase behavior and core flooding experiments at high temperatures carried out using the Guerbet alkoxy sulfates with appropriate co-surfactants show ultra-low interfacial tension, low microemulsion viscosity and high oil recoveries for target reservoir crude oil. This breakthrough in surfactant technology will both greatly increase the number of oil reservoirs where chemical EOR (surfactant-polymer, alkaline-surfactant-polymer and wettability alteration processes) is applicable and greatly improve its performance and robustness.

I dedicate this thesis to my parents

&

teachers

## ACKNOWLEDGMENTS

First and foremost, I am forever indebted for Dr. Thomas H. Kinstle, my research advisor and organic chemistry teacher for the invaluable support and guidance extended toward me to get a strong start as a graduate student. He initiated me into this challenging and fascinating field of organic chemistry. His passion for science always encouraged students to think freely, logically and motivate to try new things otherwise seemed impossible. I am truly blessed to be a member of his research group and it was an awesome learning experience. I feel honored to acknowledge his invaluable role behind this thesis.

I take this opportunity to thank my co-advisor, Dr. Upali P. Weerasooriya, for his invaluable support and assistance in joining this department and arranging facilities to carry out the surfactant part this thesis in the department of Petroleum and Geosystems Engineering, The University of Texas at Austin under his excellent supervision. I would like to thank Dr. John R. Cable and Dr. Alexander Tarnovsky for serving on my committee and for their inspiration to maintain the good work. Also I would like to thank Dr. Gary Pope at the University of Texas at Austin for allowing me to work in his laboratories.

I truly acknowledge Dr. Stephanie Adkins, for encouraging, criticizing and reviewing the research work which appears in this thesis.

It is my pleasure to thank former and present Dr. Kinstle's group members namely Krishna, Deria and others who helped me to spend friendly and collaborative time inside and outside the lab in past year.

I must thank Dr. Pope's group members Jith, Austin, Hyuntae, Dr. Kim, Chris Britton as well as Dr. Neckers' group members Leandro, Erandi, Nadeeka, Puran, Dmitry, and Saswata for facilitation me to use their scientific instruments without any hesitation.

Also I would like to thank Nora, Alita, and Mary for their administrative help in the department and Romanowicz and Dr. Chen for their technical support. Center for International Programs is highly appreciated for its help.

I want to thank BG friends Julie, Deb, Suneth, Nissanka, and Sumudu for their valuable support in making my stay in BG comfortable.

Finally, my special thank goes to my family members: my husband Sujeewa for taking worry out of my work and taking good care of me, my parents, my brothers Chamara and Chanaka, sister-in-law Asha and brother-in-law Athula. Their love, encouragement and emotional support have made me strong to complete this scientific journey in BGSU.

## TABLE OF CONTENTS

	Page
CHAPTER 1. SYNTHESIS OF DYE MATERIALS FOR DYE SENSITIZED SOLAR CELLS .....	1
1.1 Introduction.....	1
1.2 Operation of dye sensitized solar cell .....	3
CHAPTER 2. EXPERIMENTAL, RESULTS AND DISCUSSION .....	4
2.1 Synthesis pathway.....	4
2.2 Instrumentation .....	5
2.3 Material, methods and results .....	5
2.3.1 Synthesis of 5,5'-Dibromo-2,2'-bithiophene ( <b>4</b> ) .....	6
2.3.2 Synthesis of 4-(2-(5-bromo- 2,2'-bithiophenyl)ethynyl) benzaldehyde ( <b>6</b> ) .....	8
2.3.3 Synthesis of 4-(2-(5-(2-(4-(3,6-di- <i>tert</i> -butyl-9 <i>H</i> -arbazolyl)phenyl)ethynyl)-2,2'-bithiophenyl)ethynyl)benzaldehyde ( <b>8</b> ) .....	14
2.3.4 Synthesis of 2-cyano-3-(4-(2-(5-(2-(4-(3,6-di- <i>tert</i> -butyl-9 <i>H</i> -carbazolyl)phenyl)ethynyl)- 2,2'-bithiophenyl)ethynyl)phenyl)acrylic acid ( <b>1</b> ) .....	19
2.3.5 2-((4-(2-(5-(2-(4-(3,6-di- <i>tert</i> -butyl-9 <i>H</i> -carbazolyl)phenyl)ethynyl)- 2,2'-bithiophenyl)ethynyl)phenyl)methylenyl)malononitrile ( <b>2</b> ).....	26
2.4 Discussion and Conclusions .....	27
2.5 References .....	28

CHAPTER 3. Chemical Enhanced Oil Recovery .....	29
3.1 Introduction.....	29
3.1.1 Tertiary Oil Recovery.....	31
3.1.2 Background of phase behavior screening .....	35
3.1.3 Guerbet Alkoxy Sulfate Surfactants .....	42
CHAPTER 4. Experimental Methods Results and Discussion.....	45
4.1 Surfactant and Materials .....	45
4.2 Experimental Procedures .....	46
4.2.1 Sulfation of Guerbet alkoxy alcohols.....	46
4.2.2 Aqueous Solubility Experiments .....	47
4.2.3 Phase Behavior Experiments .....	48
4.2.4 ASP Core Flood Procedure .....	52
4.3 Results and Discussion .....	55
4.3.1 Phase Behavior.....	55
4.3.2 Core floods.....	62
4.4 Conclusions.....	64
4.5 References.....	66
APPENDIX. Additional NMR spectra .....	69

## LIST OF FIGURES

	Page
<b>Figure 1.1</b> A cross-section of a dye sensitized solar cell .....	2
<b>Figure 2.1</b> Mass spectrum of 5,5'-Dibromo-2,2'-bithiophene ( <b>4</b> ) .....	6
<b>Figure 2.2</b> <sup>1</sup> H spectrum of 5,5'-Dibromo-2,2'-bithiophene ( <b>4</b> ) .....	7
<b>Figure 2.3</b> Mass spectrum of 4-(2-(5-bromo- 2,2'-bithiophenyl)ethynyl) benzaldehyde ( <b>6</b> ) .....	8
<b>Figure 2.4</b> <sup>1</sup> H NMR spectrum of 4-(2-(5-bromo- 2,2'-bithiophenyl)ethynyl)benzaldehyde ( <b>6</b> ) in CDCl <sub>3</sub> .....	9
<b>Figure 2.5</b> <sup>13</sup> C NMR spectrum of 4-(2-(5-bromo- 2,2'-bithiophenyl)ethynyl)benzaldehyde ( <b>6</b> ) in CDCl <sub>3</sub> .....	10
<b>Figure 2.6</b> COSY spectrum of 4-(2-(5-bromo- 2,2'-bithiophenyl)ethynyl)benzaldehyde ( <b>6</b> ) in CDCl <sub>3</sub> .....	11
<b>Figure 2.7</b> HSQC spectrum of 4-(2-(5-bromo- 2,2'-bithiophenyl)ethynyl)benzaldehyde ( <b>6</b> ) in CDCl <sub>3</sub> .....	12
<b>Figure 2.8</b> HMBC spectrum of spectrum of 4-(2-(5-bromo-2,2'- bithiophenyl)ethynyl)benzaldehyde ( <b>6</b> ) in CDCl <sub>3</sub> .....	13
<b>Figure 2.9</b> Mass spectrum of 4-(2-(5-(2-(4-(3,6-di- <i>tert</i> -butyl-9 <i>H</i> - carbazolyl)phenyl)ethynyl)- 2,2'-bithiophenyl)ethynyl)benzaldehyde ( <b>8</b> ).....	14
<b>Figure 2.10</b> <sup>1</sup> H NMR of 4-(2-(5-(2-(4-(3,6-di- <i>tert</i> -butyl-9 <i>H</i> -carbazolyl)phenyl)ethynyl)- 2,2'-bithiophenyl)ethynyl)benzaldehyde ( <b>8</b> ) in CDCl <sub>3</sub> .....	15
<b>Figure 2.11</b> <sup>13</sup> C NMR of 4-(2-(5-(2-(4-(3,6-di- <i>tert</i> -butyl-9 <i>H</i> -carbazolyl)phenyl)ethynyl)- 2,2'-bithiophenyl)ethynyl)benzaldehyde ( <b>8</b> ) in CDCl <sub>3</sub> .....	16

- Figure 2.12** COSY spectrum of 4-(2-(5-(2-(4-(3,6-di-*tert*-butyl-9*H*-carbazolyl)phenyl)ethynyl)-2,2'-bithiophenyl)ethynyl)benzaldehyde (8) in CDCl<sub>3</sub>..... 17
- Figure 2.13** HSQC spectrum of 4-(2-(5-(2-(4-(3,6-di-*tert*-butyl-9*H*-carbazolyl)phenyl)ethynyl)-2,2'-bithiophene)ethynyl)benzaldehyde (8) in CDCl<sub>3</sub>..... 18
- Figure 2.14** Mass spectrum of 2-cyano-3-(4-(2-(5-(2-(4-(3,6-di-*tert*-butyl-9*H*-carbazolyl)phenyl)ethynyl)-2,2'-bithiophenyl)ethynyl)phenyl)acrylic acid (1)
- Figure 2.15** <sup>1</sup>H NMR of 2-cyano-3-(4-(2-(5-(2-(4-(3,6-di-*tert*-butyl-9*H*-carbazolyl)phenyl)ethynyl)-2,2'-bithiophenyl)ethynyl)phenyl)acrylic acid (1) in DMSO..... 20
- Figure 2.16** <sup>13</sup>C NMR of 2-cyano-3-(4-(2-(5-(2-(4-(3,6-di-*tert*-butyl-9*H*-carbazolyl)phenyl)ethynyl)-2,2'-bithiophenyl)ethynyl)phenyl)acrylic acid (1) in DMSO..... 21
- Figure 2.17** COSY spectrum of 2-cyano-3-(4-(2-(5-(2-(4-(3,6-di-*tert*-butyl-9*H*-carbazolyl)phenyl)ethynyl)-2,2'-bithiophenyl)ethynyl)phenyl)acrylic acid (1) in DMSO (600MHz)..... 22
- Figure 2.18** HSQC spectrum of 2-cyano-3-(4-(2-(5-(2-(4-(3,6-di-*tert*-butyl-9*H*-carbazolyl)phenyl)ethynyl)-2,2'-bithiophenyl)ethynyl)phenyl)acrylic acid (1) in DMSO (600MHz)..... 23
- Figure 2.19.** HMBC spectrum of 2-cyano-3-(4-(2-(5-(2-(4-(3,6-di-*tert*-butyl-9*H*-carbazolyl)phenyl)ethynyl)-2,2'-bithiophenyl)ethynyl)phenyl)acrylic acid (1) in DMSO (600MHz)..... 24

<b>Figure 2.20</b> Absorbance and fluorescence spectra of <b>1</b> , $\lambda_{\text{ex}} = 425 \text{ nm}$ .....	25
<b>Figure 2.21</b> Mass spectrum of 2-((4-(2-(5-(2-(4-(3,6-di- <i>tert</i> -butyl-9 <i>H</i> - carbazolyl)phenyl)ethynyl)-2,2'- bithiophenyl)ethynyl)phenyl)methylenyl)malononitrile ( <b>2</b> ).....	26
<b>Figure 3.1</b> Water flooding through a cavity completely filled with oil.....	30
<b>Figure 3.2</b> Oil in a capillary after water flooding.....	31
<b>Figure 3.3</b> Surfactant flooding through a cavity with filled with oil.....	32
<b>Figure 3.4</b> Surfactant flooding forming oil bank in the cavity.....	33
<b>Figure 3.5</b> Winsor surfactant phase behavior categories.....	35
<b>Figure 3.6</b> Microemulsion phase behavior as a function of salinity with one pipette tilted	
<b>Figure 3.7</b> Pipette from a microemulsion phase behavior salinity scan experiment being inverted .....	38
<b>Figure 3.8</b> Schematic capillary desaturation curve .....	41
<b>Figure 3.9</b> Synthesis scheme for Guerbet alkoxy alcohol with PO and EO groups.....	44
<b>Figure 4.1</b> Structures of two sulfonates in $\text{C}_{20-24}$ IOS .....	46
<b>Figure 4.2</b> Sulfation reaction of Guerbet alkoxy alcohol .....	46
<b>Figure 4.3</b> #1 and #2 ASP flood set-up.....	54
<b>Figure 4.4</b> Solubilization ratio as a function of sodium carbonate concentration for 10% crude oil #1 and the formulations of experiment 23 at 85 °C.....	57
<b>Figure 4.5</b> Solubilization ratio as a function of sodium carbonate concentration for 20% crude oil #1 and the formulations of experiment 23 at 85 °C.....	57
<b>Figure 4.6</b> Solubilization ratio as a function of sodium carbonate concentration for 30% crude oil #1 and the formulations of experiment 23 at 85 °C.....	58

<b>Figure 4.7</b> Solubilization ratio as a function of sodium carbonate concentration for 40% crude oil #1 and the formulations of experiment 23 at 85 °C .....	58
<b>Figure 4.8</b> Solubilization ratio as a function of sodium carbonate concentration for 50% crude oil #1 and the formulations of experiment 23 at 85 °C .....	59
<b>Figure 4.9</b> Solubilization ratio as a function of sodium carbonate concentration for 10% crude oil #1 and the formulations of experiment 24 at 85 °C .....	60
<b>Figure 4.10</b> Solubilization ratio as a function of sodium carbonate concentration for 20% crude oil #1 and the formulations of experiment 24 at 85 °C .....	60
<b>Figure 4.11</b> Solubilization ratio as a function of sodium carbonate concentration for 30% crude oil #1 and the formulations of experiment 24 at 85 °C .....	61
<b>Figure 4.12</b> Solubilization ratio as a function of sodium carbonate concentration for 40% crude oil #1 and the formulations of experiment 24 at 85 °C .....	61
<b>Figure 4.13</b> Hydrolysis of MA 80-I in basic medium .....	62
<b>Figure 4.14</b> Oil Recovery data for core flood #1 .....	63
<b>Figure 4.15</b> Oil Recovery data for core flood #2 .....	64

## LIST OF TABLES

	Page
<b>Table 4.1</b> Description of Crude Oil.....	50
<b>Table 4.2</b> Composition of Synthetic Brine (SB) and Synthetic Soften Brine (SSB) .....	50
<b>Table 4.3</b> Formulations used for Phase Behavior Screening .....	51
<b>Table 4.4</b> Core Properties of Core flood #1 .....	53
<b>Table 4.5</b> Core Properties of Core flood #2 .....	54

## CHAPTER 1

### Synthesis of dye materials for dye sensitized solar cells

#### 1.1. Introduction

An impending energy crisis is one of the most important topics in the present era because existing fossil fuels sources used for energy generation are rapidly depleting.

Regeneration of these sources would require millions of years. Some scientists predict that existing fossil fuel resources will be consumed in less than 50 years if usage follows the present trends. Nuclear, solar, wind and hydroelectric are considered as the main alternatives for fossil fuels. When current generation efficiency, environmental pollution, risk, and cost are considered, all are currently too expensive, but solar energy is the best candidate to replace fossil fuel in the long term.<sup>1</sup>

Solar energy is a renewable energy source. Considering the abundance of solar radiation reaching the earth which is approximately 120,000 TW compared to a current global consumption of 13 TW, solar energy alone offers a satisfactory energy source if cost-effective solar cell technologies can be successfully developed and implemented.

Currently available solar cells can be categorized into three groups: silicon bulk heterojunction cells (first-generation technology); thin film (CuInGaSe<sub>2</sub> [CIGS], CdTe) solar cells (second-generation); and dye-sensitized solar cells (DSSC or DSC) (third-generation).<sup>2</sup> Silicon based solar cells still dominate the solar energy market but its rapid expansion has been limited due to the high cost of solar-grade silicon production and processing. Thin film based solar cells have entered the market but application has been limited since they incorporate very toxic materials like Cadmium.

Dye-sensitized solar cells are a relatively new class of low-cost solar cell, that belong to the thin film group of solar cells. They are based on a semiconductor formed between a photo-sensitized anode and an electrolyte, a *photoelectrochemical* system. This cell concept was invented by Michael Grätzel and Brian O'Regan at the École Polytechnique Fédérale de Lausanne in 1991 and they are known as Grätzel cells.<sup>3,4</sup> This cell is extremely promising because it is made of low-cost materials and does not need elaborate apparatus to manufacture. In bulk, it should be significantly less expensive than older solid-state cell designs. It can be engineered into flexible sheets and is mechanically robust, requiring no protection from minor events like hail . Although its conversion efficiency is less than that of the best thin-film cells, its price-performance ratio ( $\text{kWh}/(\text{m}^2 \cdot \text{annum} \cdot \text{dollar})$ ) should be high enough to allow it to compete with fossil fuel electrical generation (grid parity).<sup>5</sup> Commercial applications, which are currently complicated due to chemical stability problems, are now forecast in the European Union Photovoltaic Roadmap to be a potentially significant contributor to renewable electricity generation by 2020.<sup>6</sup>

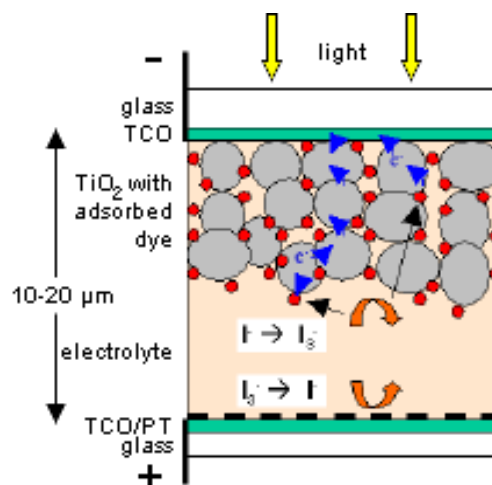


**Figure 1.1.** A cross-section of a dye sensitized solar cell.

## 1.2. Operation of dye sensitized solar cell

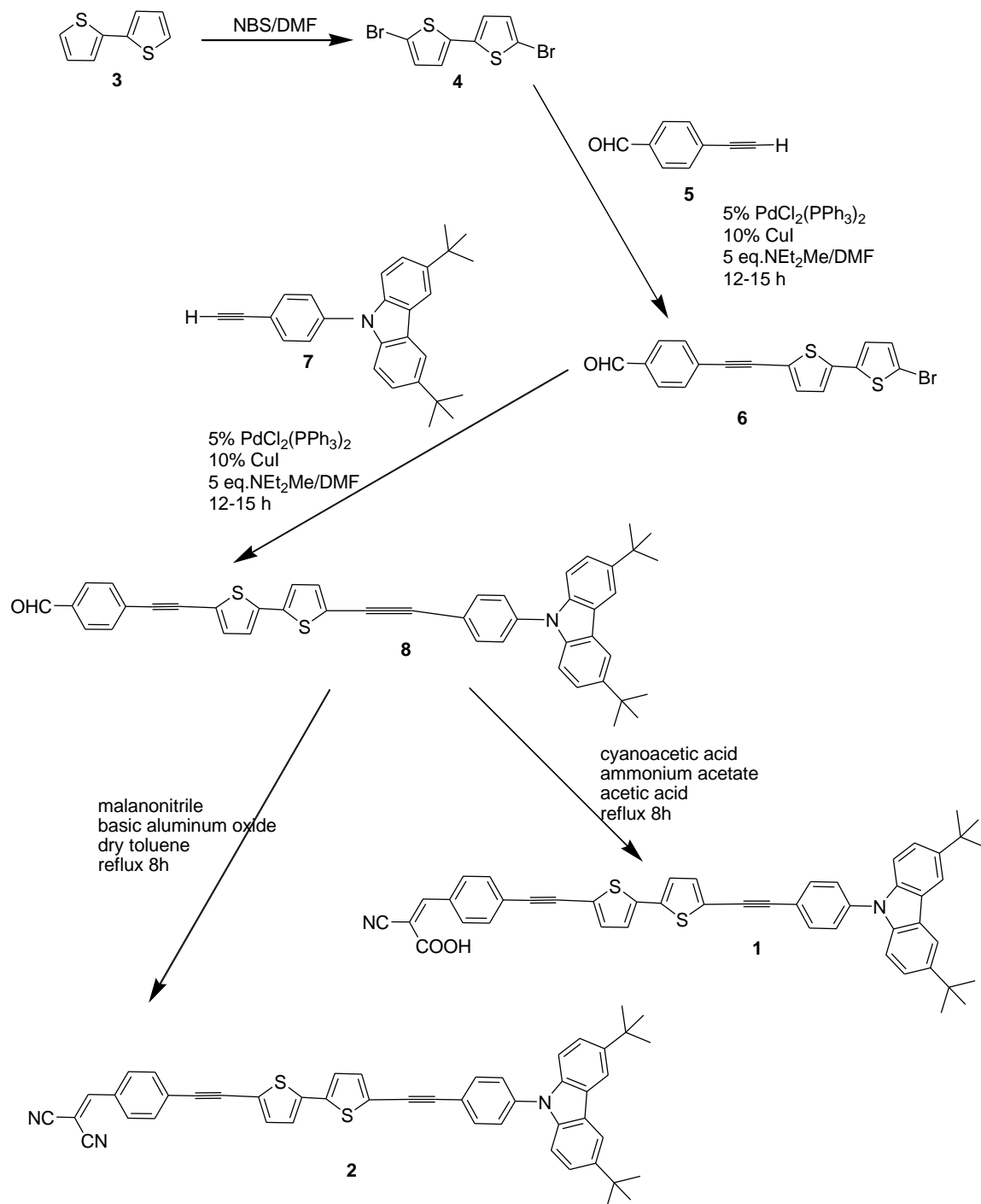
In the first generation cell, the silicon acts as both the source of photoelectrons, as well as providing the electric field to separate the charges and create a current. Dye-sensitized solar cells separate the two functions provided by silicon in a traditional cell design. In the dye-sensitized solar cell, the bulk of the semiconductor is used solely for charge transport, and the photoelectrons are provided from a separate photosensitive dye. These dye molecules must contain terminal anchoring groups such as  $-\text{COO}^-$  or  $-\text{SCN}^-$  to chemisorb the chromophore to the conductive  $\text{TiO}_2$  electrode layer. Charge separation occurs at the surfaces between the dye, semiconductor and electrolyte.<sup>5</sup> Another important property of the dye material is able to absorb photons in the visible and IR region because  $\text{TiO}_2$  band gap excitation by UV light generates electrons and holes which are easily accepted by oxygen atoms to form peroxides. These peroxides rapidly degrade the coated dye material especially when liquid electrolytes are present.<sup>7</sup>

The useful dye molecules are quite small (nanometer sized), so in order to capture a reasonable amount of the incoming light the layer of dye molecules needs to be made fairly thick, much thicker than the molecules themselves. To address this problem, a nanomaterial is used as a scaffold to hold large numbers of the dye molecules in a 3-D matrix, increasing the number of molecules for any given surface area of cell. In existing designs, this scaffolding is provided by the semiconductor material, which serves a dual purpose.

## CHAPTER 2

## Experimental, result and discussion

## 2.1. Synthesis Pathway



## 2.2. Instrumentation.

$^1\text{H}$  NMR,  $^{13}\text{C}$  NMR, and 2D NMR spectra were recorded using Bruker 300 MHz and 500 MHz spectrometers.  $\text{CDCl}_3$  and  $\text{DMSO-d}_6$  were used as the solvents for NMR and chemical shifts were measured relative to tetramethylsilane (TMS) and solvent. Mass spectra were recorded using a Shimadzu GCMS-QP5050A instrument equipped with an electron bombardment probe (70 eV). Matrix assisted laser desorption ionization (MALDI) spectra were obtained using a Bruker Deltonic Omniflex instrument ( $\text{N}_2$  laser, 337 nm).

## 2.3. Materials, methods and results

All reagents, solvents, 2,2'-bithiophene and 4-ethynylbenzaldehyde were purchased from Aldrich. All chemicals were used without further purification unless otherwise noted. Compound **7** was pre-synthesized in our lab by another student.

### 2.3.1. Synthesis of 5,5'-Dibromo-2,2'-bithiophene (4)

5,5'-Dibromo-2,2'-bithiophene was synthesized following a literature method<sup>1</sup>. *N*-Bromosuccinimide (NBS) (11.03 g, 0.062 mol) was added portionwise at 0 °C to a solution of bithiophene (5.0g ,0.036 mol) in *N,N*-dimethylformamide, DMF(30 ml) in the absence of light. After stirring for 3 h at room temperature, the reaction mixture was poured onto ice and the white precipitate was filtered and dried using a vacuum oven.<sup>8</sup> The precipitate was recrystallized using absolute EtOH to yield **4** as a white solid; Yield 8.43 g (86.7%).  $M^+$ (m/z) 322.

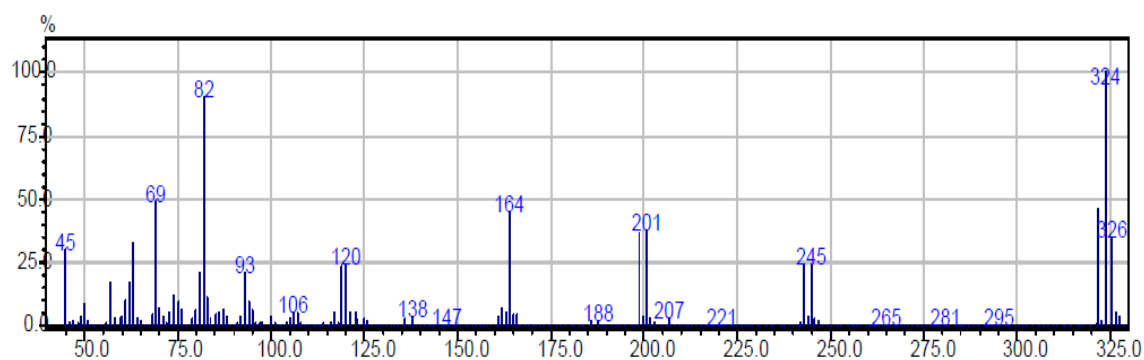


**Figure 2.1.** Mass spectrum of 5,5'-Dibromo-2,2'-bithiophene (**4**).

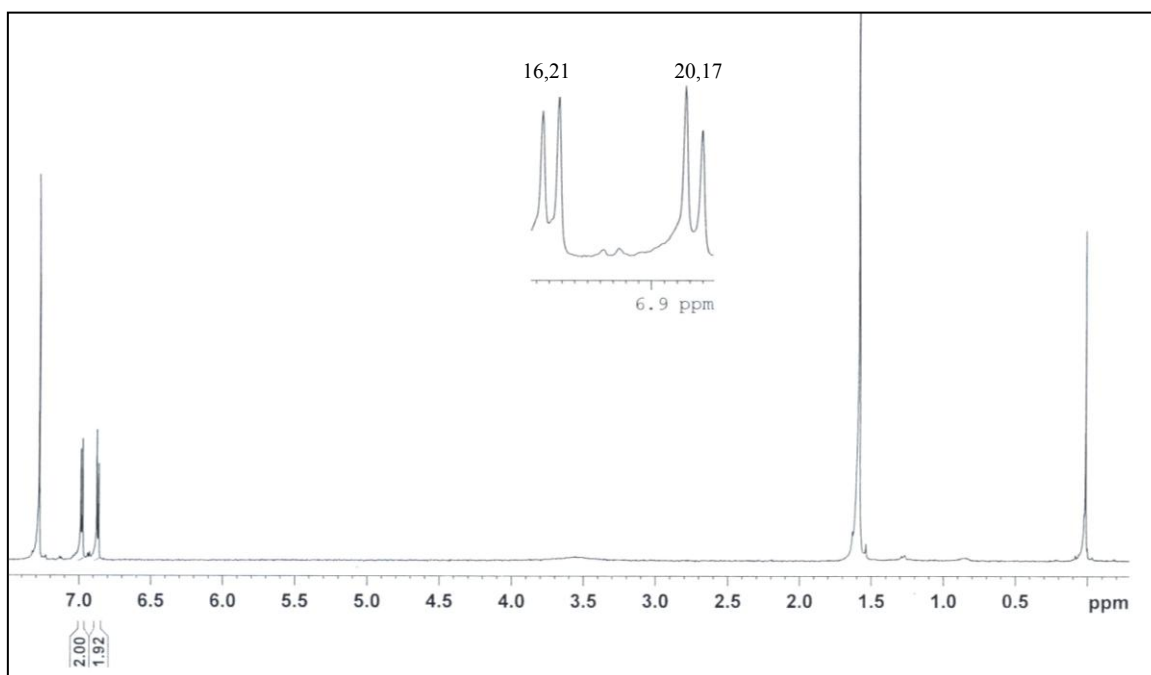
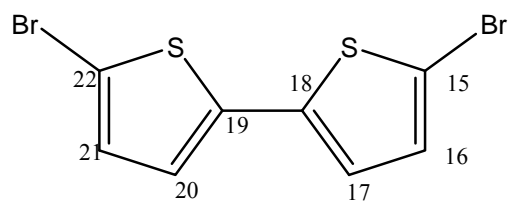


**Figure 2.2.** <sup>1</sup>H NMR spectrum of 5,5'-Dibromo-2,2'-bithiophene (**4**).

### 2.3.2. Synthesis of 4-(2-(5-bromo-2,2'-bithiophenyl)ethynyl)benzaldehyde (**6**).

5,5'-Dibromo-2,2'-bithiophene (**4**) (0.45g, 1.38 mmol), PdCl<sub>2</sub>(PPh<sub>3</sub>)<sub>2</sub> (16 mg), CuI (12mg) isopropyl ethyl amine (1 ml) and DMF (9 ml) were mixed together in a 100 ml round bottom flask and argon was bubbled through the mixture for 20 minutes. Then 4-ethynylbenzaldehyde (0.1 g, 0.77 mmol) was added and the mixture was stirred 15 h at 80 °C under argon. The reaction mixture was poured into distilled water and extracted with DCM. The extract was washed with 0.5 M HCl twice, then with saturated NaHCO<sub>3</sub> and finally with distilled water. This solution was dried using anhydrous NaSO<sub>4</sub>, and pentane (1/3 volume of DCM) was added. The resultant solution was filtered using a Buchner funnel containing layer of silica. The filtrate was concentrated under vacuum and the crude product was purified by flash chromatography (silica gel, 30% DCM in hexane) to obtain pure **6** (0.17g 65%). M<sup>+</sup>(m/z) 372.

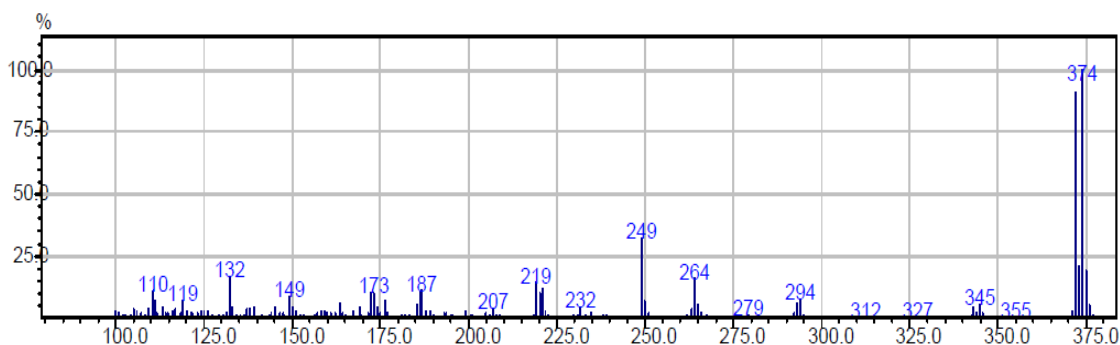


**Figure 2.3.** Mass spectrum of 4-(2-(5-bromo-2,2'-bithiophenyl)ethynyl)benzaldehyde (**6**).

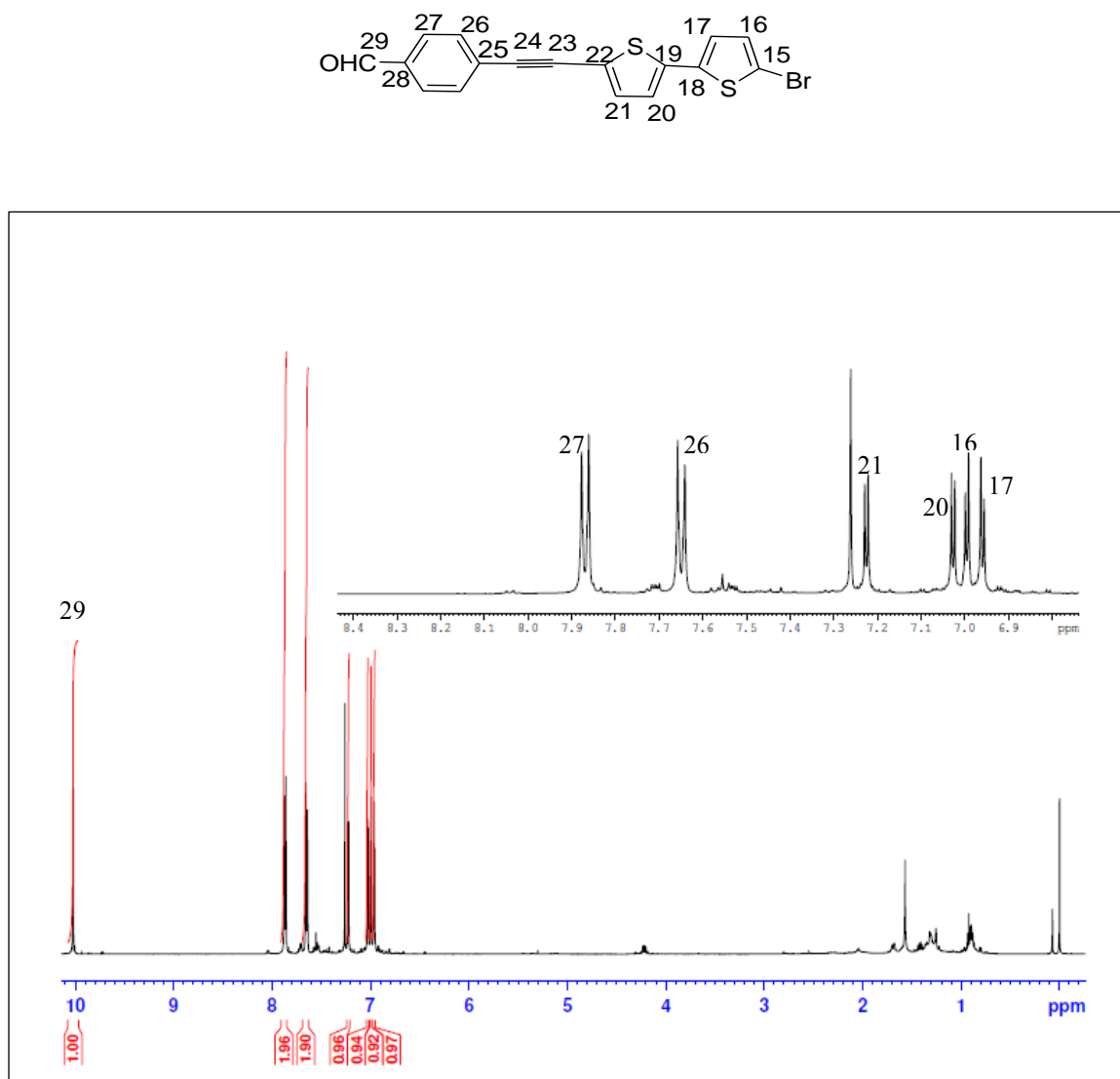


**Figure 2.4.** <sup>1</sup>H NMR spectrum of 4-(2-(5-bromo-2,2'-bithiophenyl)ethynyl)benzaldehyde (**6**) in CDCl<sub>3</sub>.

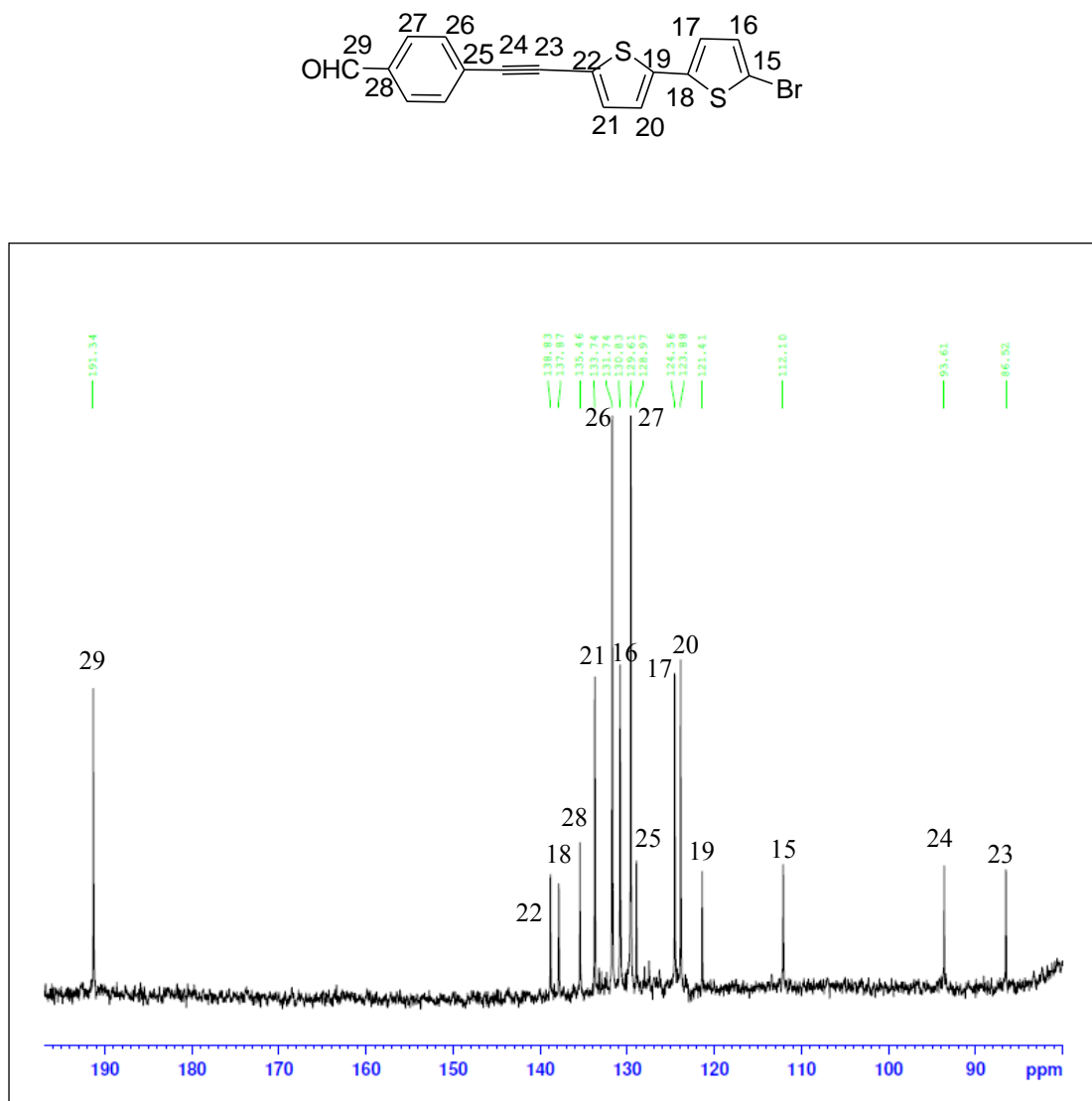


**Figure 2.5.**  $^{13}\text{C}$  NMR spectrum of 4-(2-(5-bromo-2,2'-bithiophenyl)ethynyl)benzaldehyde (6) in  $\text{CDCl}_3$ .

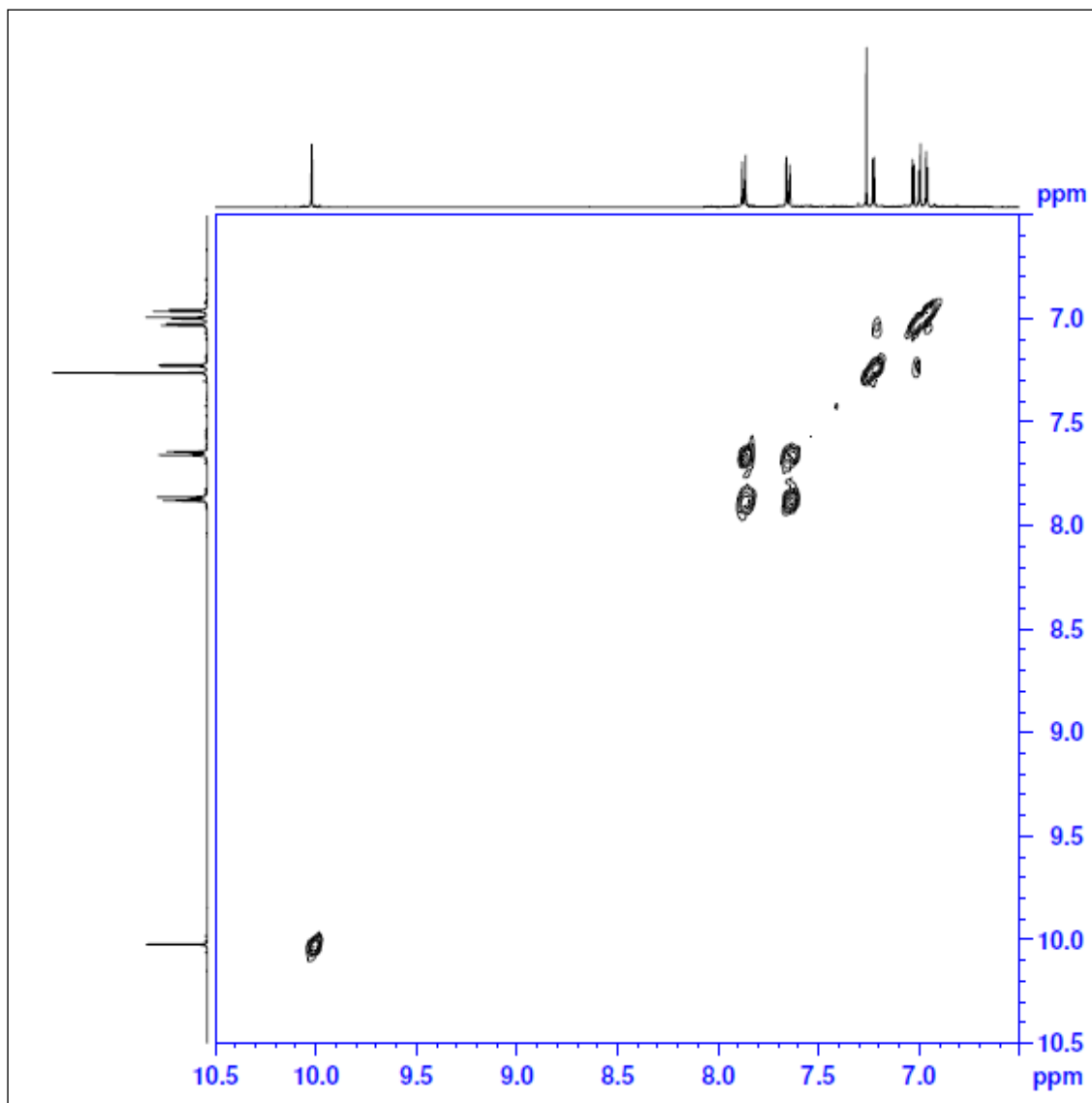


**Figure 2.6.** COSY spectrum of 4-(2-(5-bromo-2,2'-bithiophenyl)ethynyl)benzaldehyde (**6**) in CDCl<sub>3</sub>.

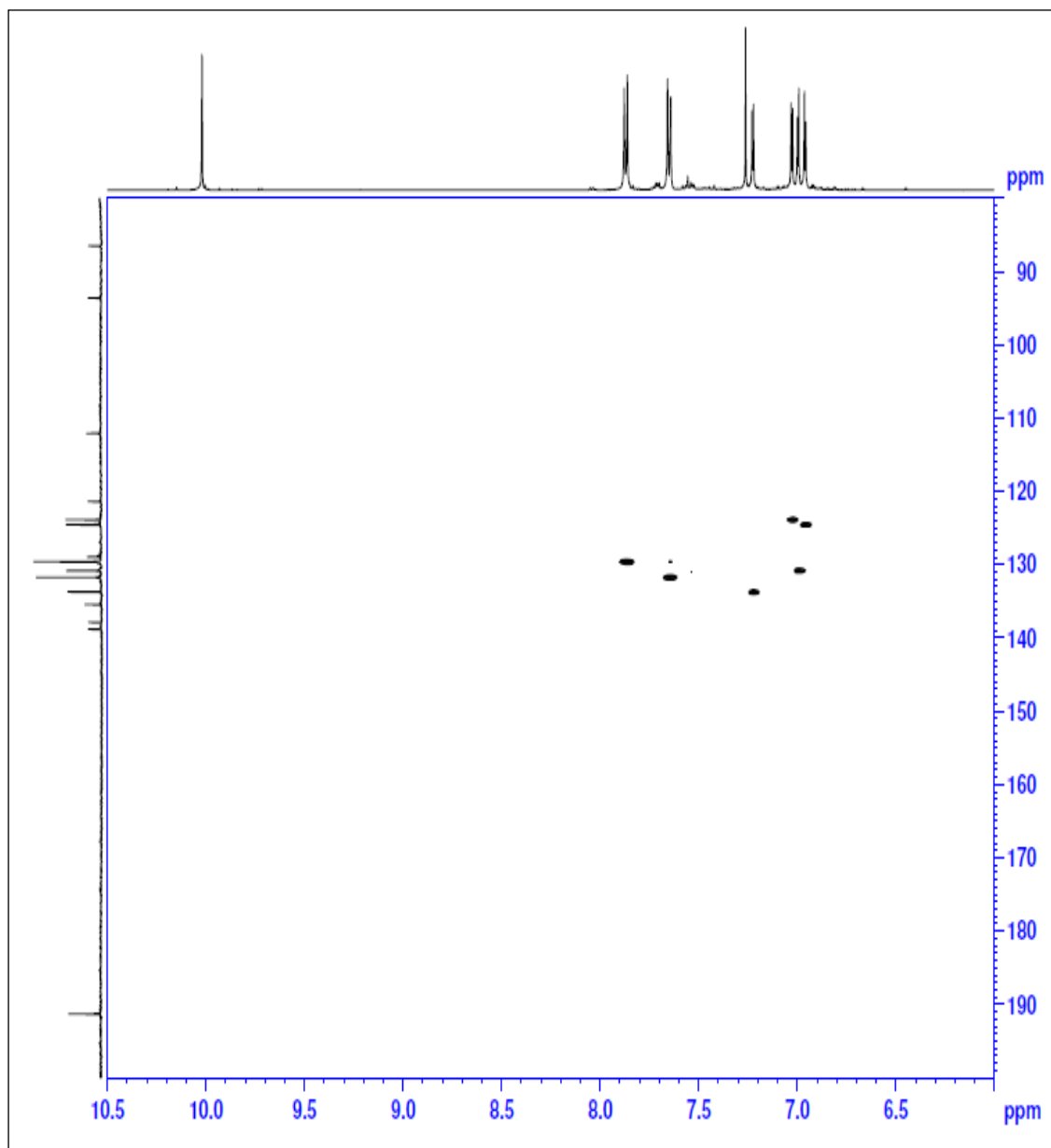


**Figure 2.7.** HSQC spectrum of 4-(2-(5-bromo- 2,2'-bithiophenyl)ethynyl)benzaldehyde (**6**) in  $\text{CDCl}_3$ .

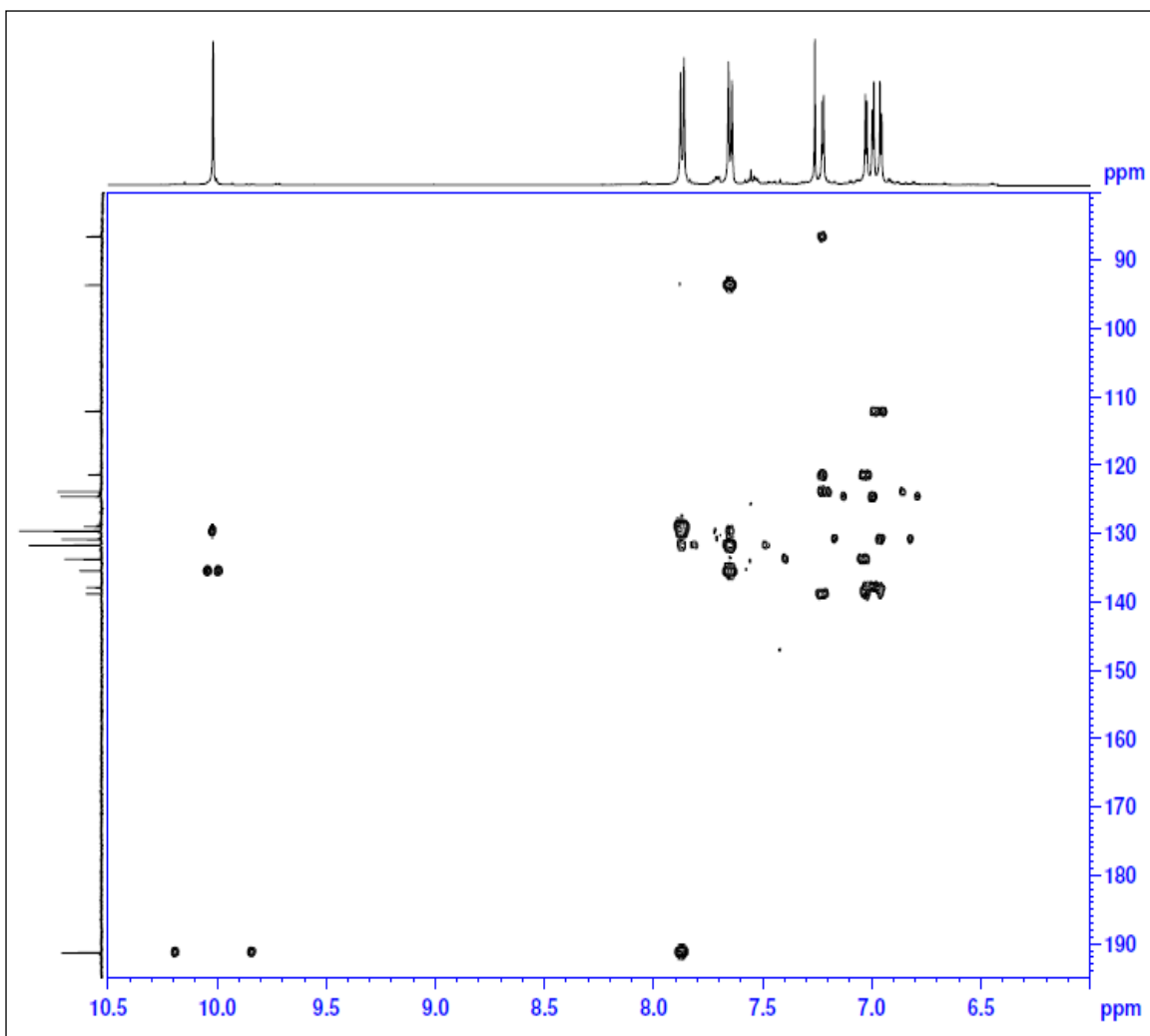


**Figure 2.8.** HMBC spectrum of spectrum of 4-(2-(5-bromo-2,2'-bithiophenyl)ethynyl)benzaldehyde (**6**) in  $\text{CDCl}_3$ .

### 2.3.3. Synthesis of 4-(2-(5-(2-(4-(3,6-di-*tert*-butyl-9*H*-carbazolyl)phenyl)ethynyl)-2,2'-bithiophenyl)ethynyl)benzaldehyde (**8**)

Compound **6** (100mg, 0.269mmol), PdCl<sub>2</sub>(PPh<sub>3</sub>)<sub>2</sub> (6.7 mg), CuI (5.1mg), isopropyl ethyl amine (0.5 ml) and DMF (7 ml) were mixed in a 100ml round bottom flask. Argon was bubbled through the mixture for 20 minutes. After that compound **7** (0.1 g, 0.77 mmol) was added and stirred for 15 h at 80 °C under argon. After the usual workup, the solvent was evaporated using vacuum and the crude product was recrystallized from DCM and hexane to obtain pure **8** (0.15g, 82%). MALDI M<sup>+</sup> (m/z) 671.

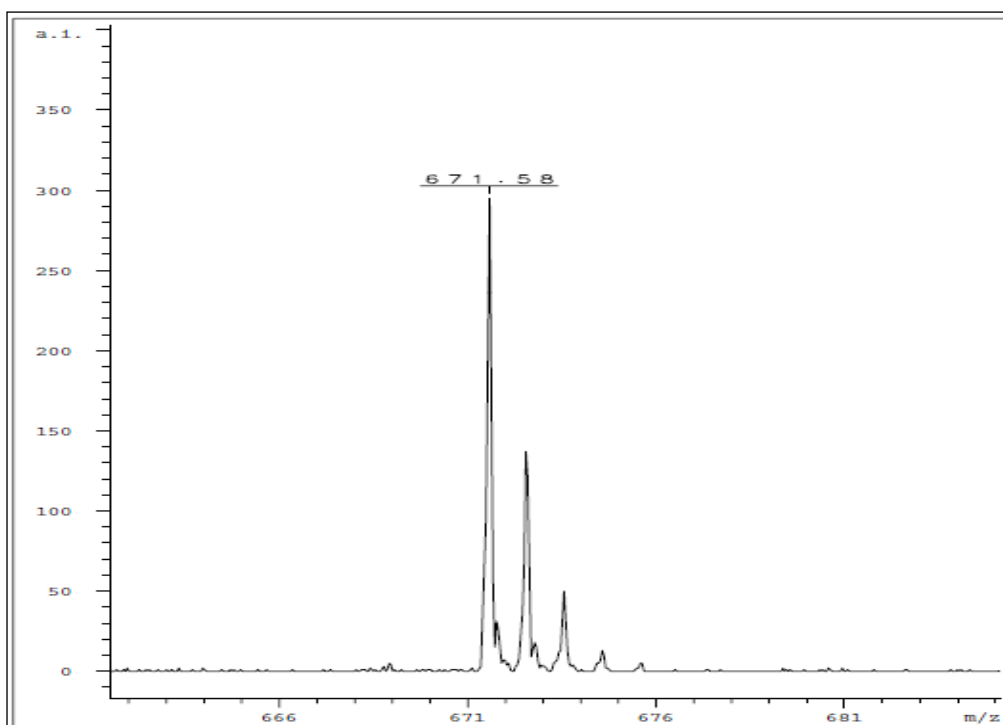


**Figure 2.9.** Mass spectrum of 4-(2-(5-(2-(4-(3,6-di-*tert*-butyl-9*H*-carbazolyl)phenyl)ethynyl)-2,2'-bithiophenyl)ethynyl)benzaldehyde (**8**).

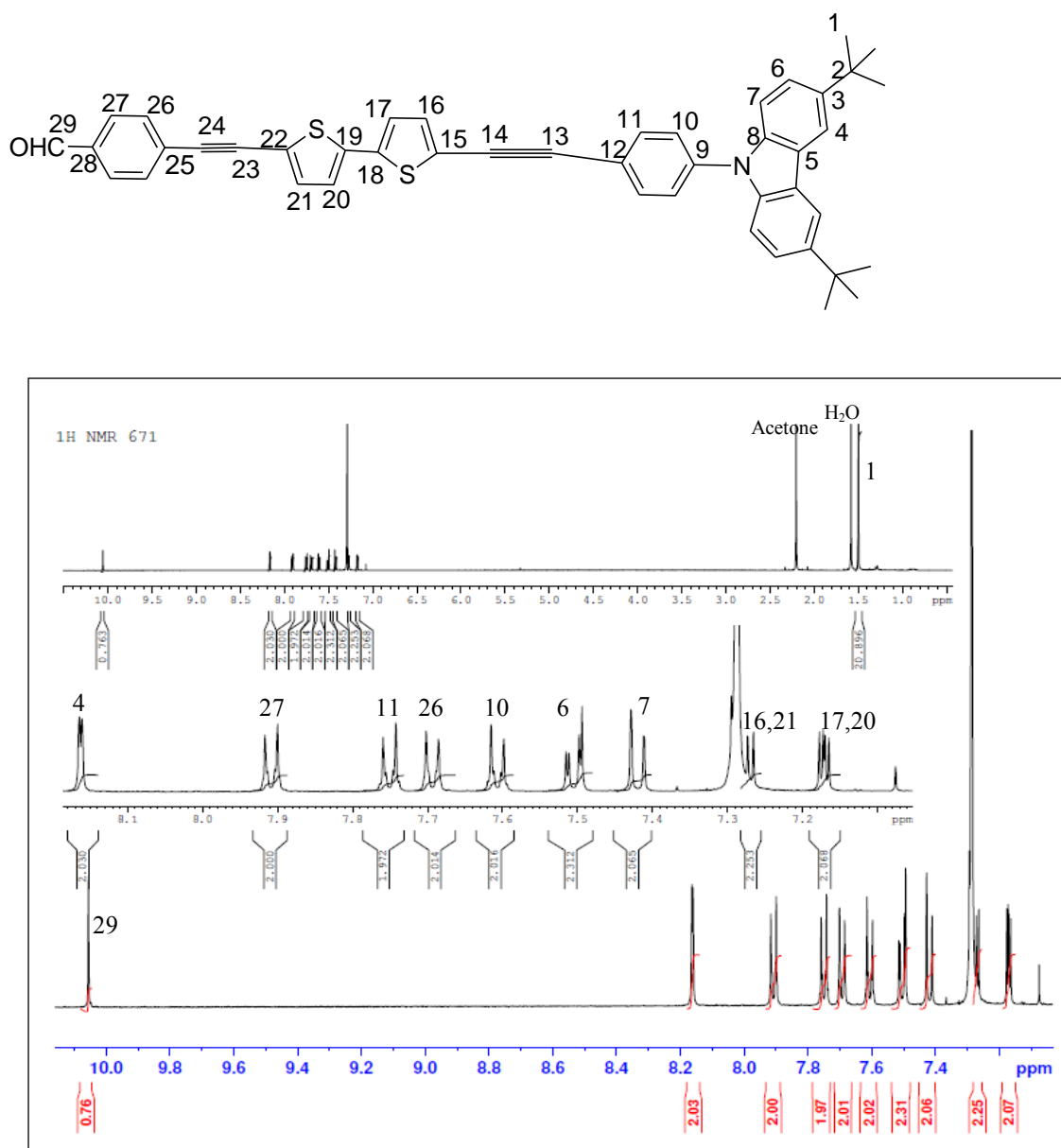


**Figure 2.10.**  $^1\text{H}$  NMR of 4-(2-(5-(2-(4-(3,6-di-*tert*-butyl-9H-carbazolyl)phenyl)ethynyl)-2,2'-bithiophenyl)ethynyl)benzaldehyde (**8**) in  $\text{CDCl}_3$ .

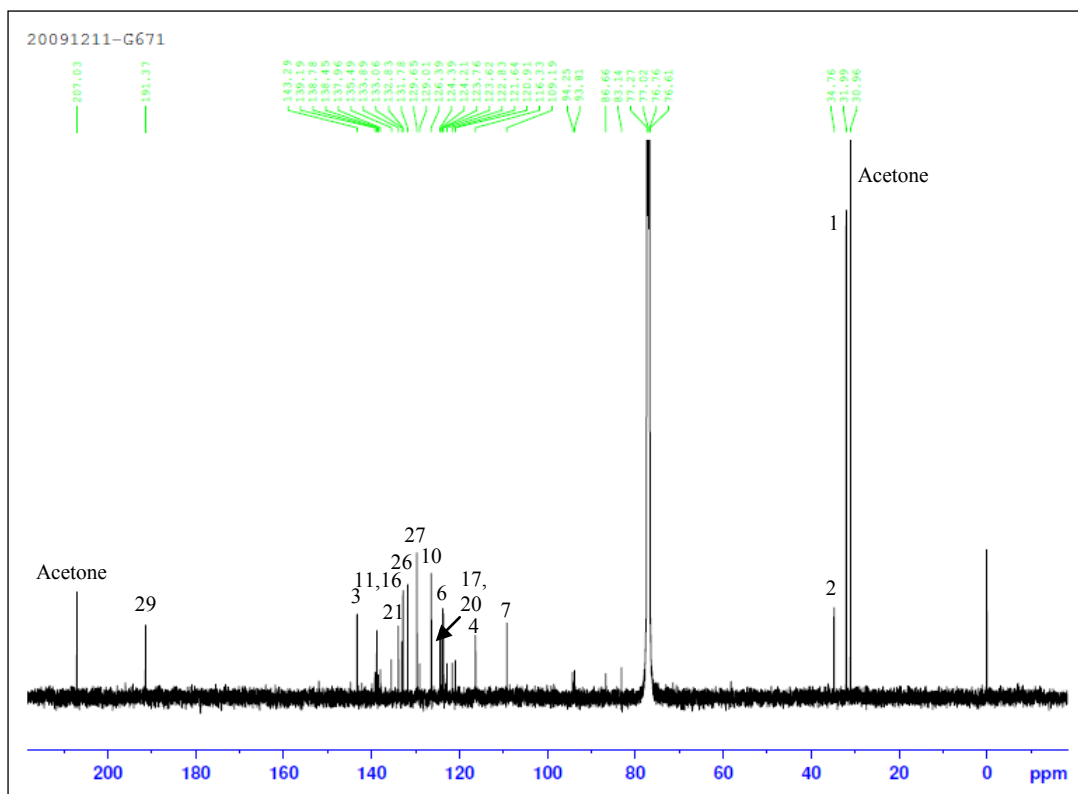


**Figure 2.11.**  $^{13}\text{C}$  NMR of 4-(2-(5-(2-(4-(3,6-di-*tert*-butyl-9*H*-carbazolyl)phenyl)ethynyl)-2,2'-bithiophenyl)ethynyl)benzaldehyde (**8**) in  $\text{CDCl}_3$ .

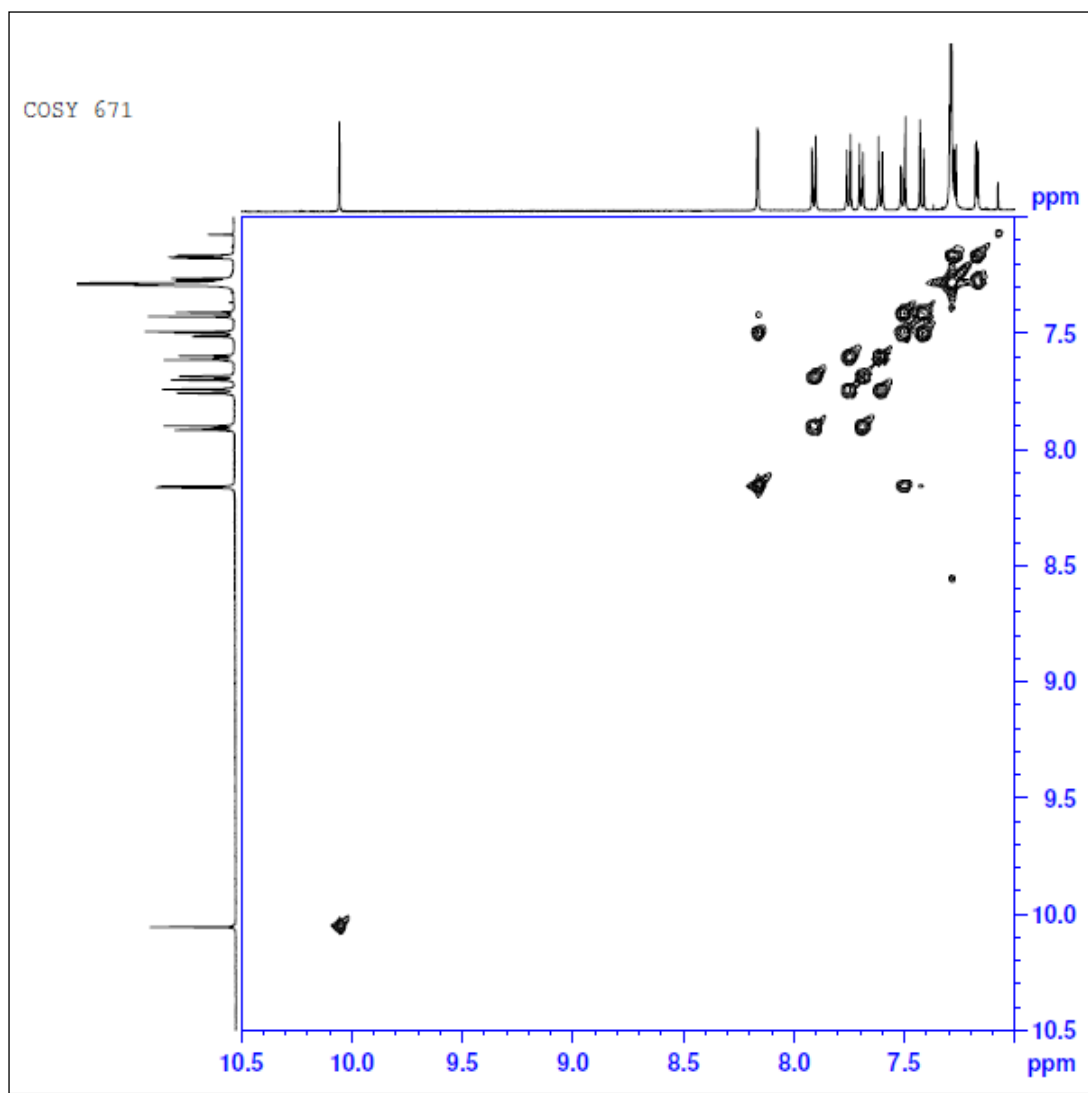


**Figure 2.12.** COSY spectrum of 4-(2-(5-(2-(4-(3,6-di-*tert*-butyl-9*H*-carbazolyl)phenyl)ethynyl)-2,2'-bithiophenyl)ethynyl)benzaldehyde (**8**) in CDCl<sub>3</sub>.

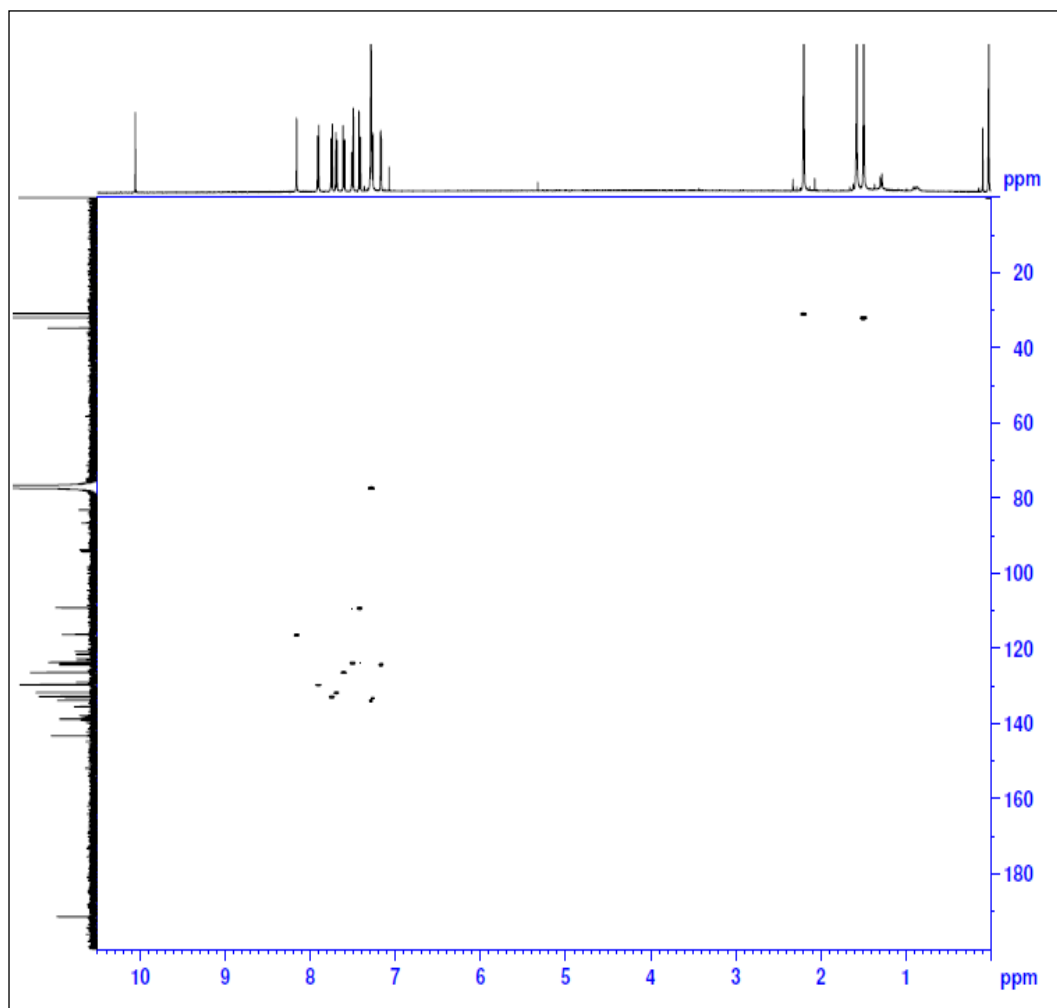


**Figure 2.13.** HSQC spectrum of 4-(2-(5-(2-(4-(3,6-di-*tert*-butyl-9*H*-carbazolyl)phenyl)ethynyl)-2,2'-bithiophenyl)ethynyl)benzaldehyde (**8**) in  $\text{CDCl}_3$ .

**2.3.4. Synthesis of 2-cyano-3-(4-(2-(5-(2-(4-(3,6-di-*tert*-butyl-9*H*-carbazolyl)phenyl)ethynyl)-2,2'-bithiophenyl)ethynyl)phenyl)acrylic acid (1)**

Compound **8** (150mg, 0.223 mmol) , cyanoacetic acid (9ml), ammonium acetate (0.05g) and acetic acid (10 ml) were added into a 50 ml two necked round bottom flask. This mixture was refluxed under argon for 8 h and allowed to cool to room temperature. The resultant solid was filtered and washed with distilled water, diethyl ether and methanol to yield a bright red solid (142mg,86%).  $M^+(m/z)$  738.

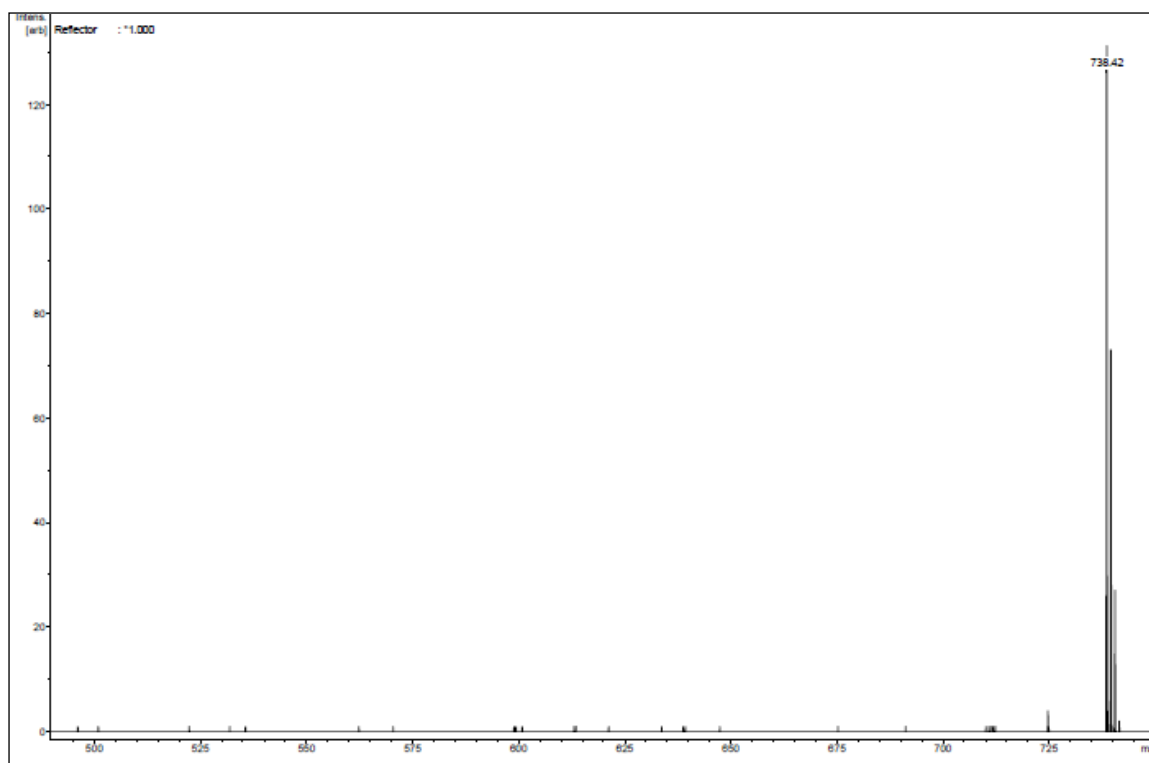


**Figure 2.14.** Mass spectrum of 2-cyano-3-(4-(2-(5-(2-(4-(3,6-di-*tert*-butyl-9*H*-carbazolyl)phenyl)ethynyl)-2,2'-bithiophenyl)ethynyl)phenyl)acrylic acid (**1**).

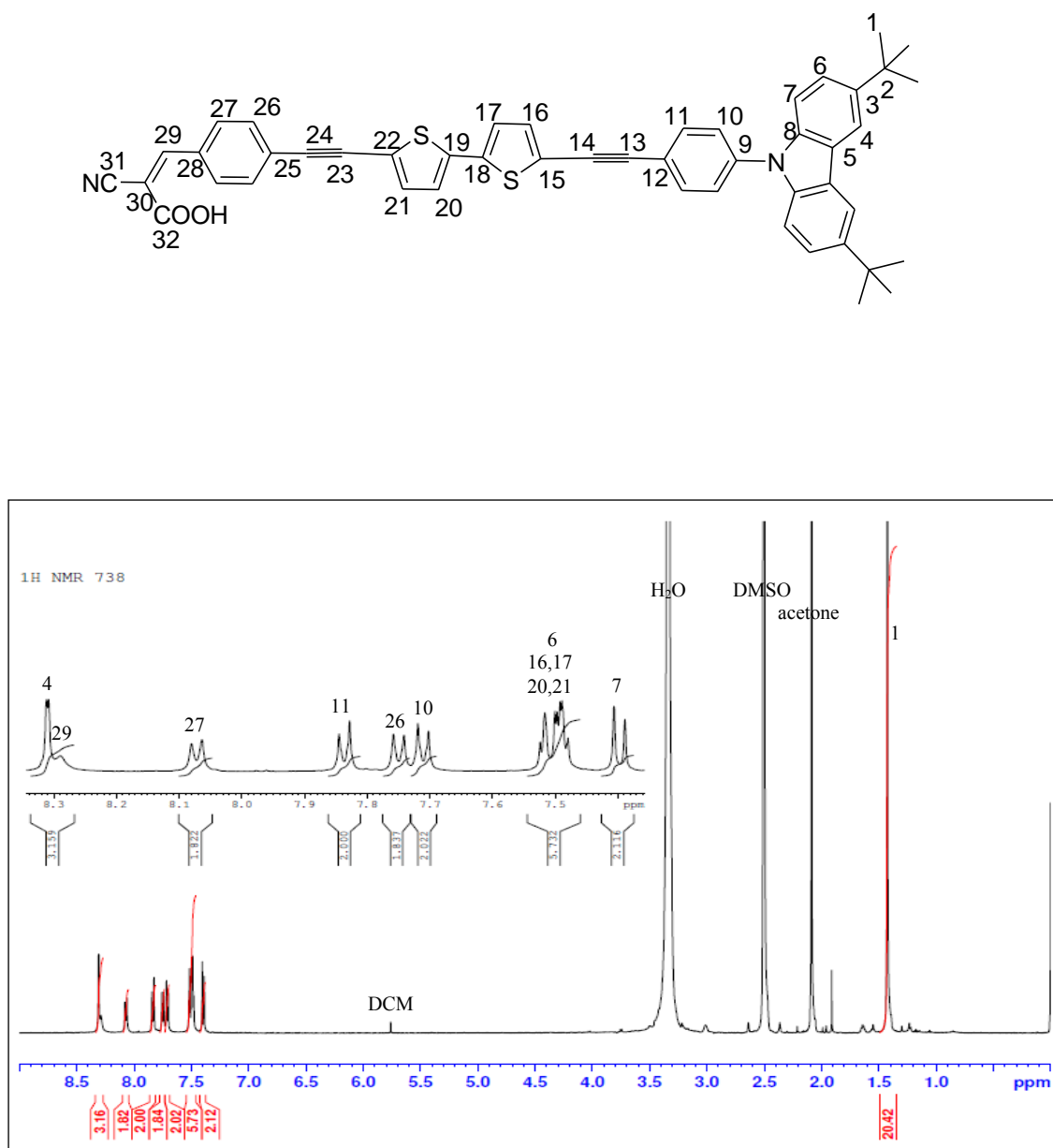


**Figure 2.15.** <sup>1</sup>H NMR of 2-cyano-3-(4-(2-(5-(2-(4-(3,6-di-*tert*-butyl-9H-carbazolyl)phenyl)ethynyl)-2,2'-bithiophenyl)ethynyl)phenyl)acrylic acid (**1**) in DMSO.

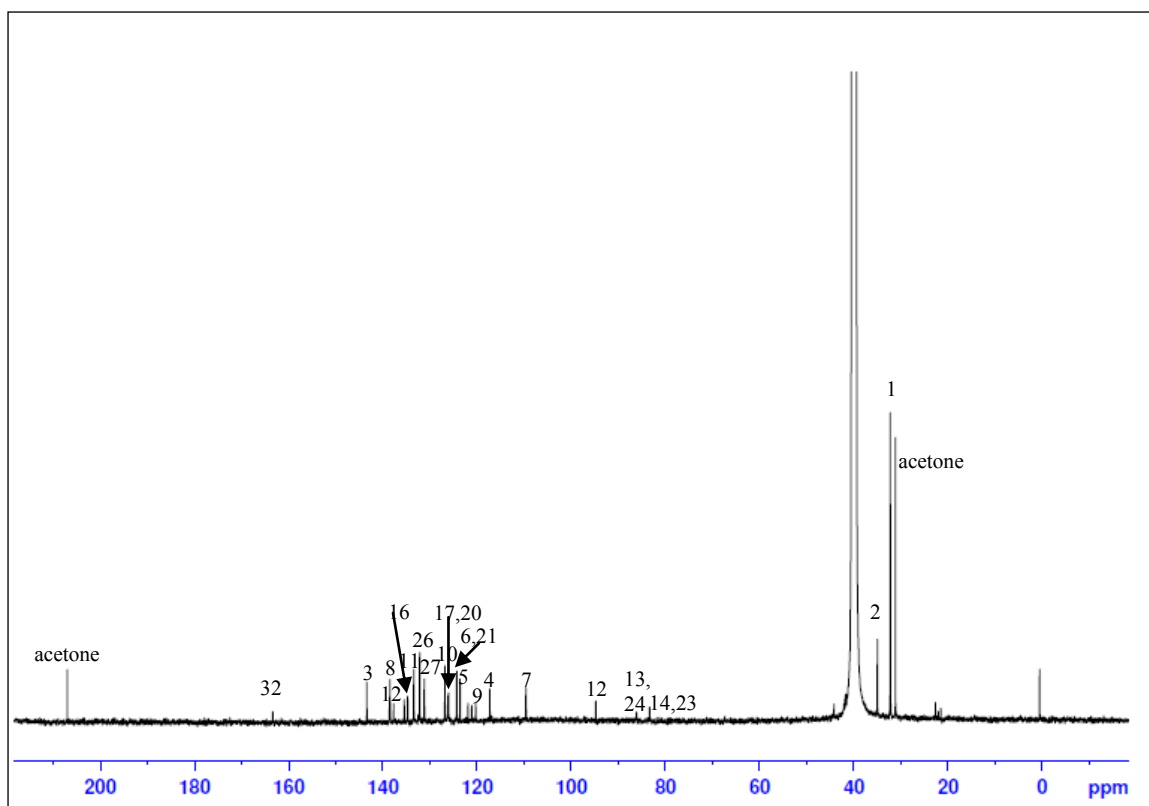


**Figure 2.16.**  $^{13}\text{C}$  NMR of 2-cyano-3-(4-(2-(5-(2-(4-(3,6-di-*tert*-butyl-9*H*-carbazolyl)phenyl)ethynyl)-2,2'-bithiophenyl)ethynyl)phenyl)acrylic acid (**1**) in DMSO.

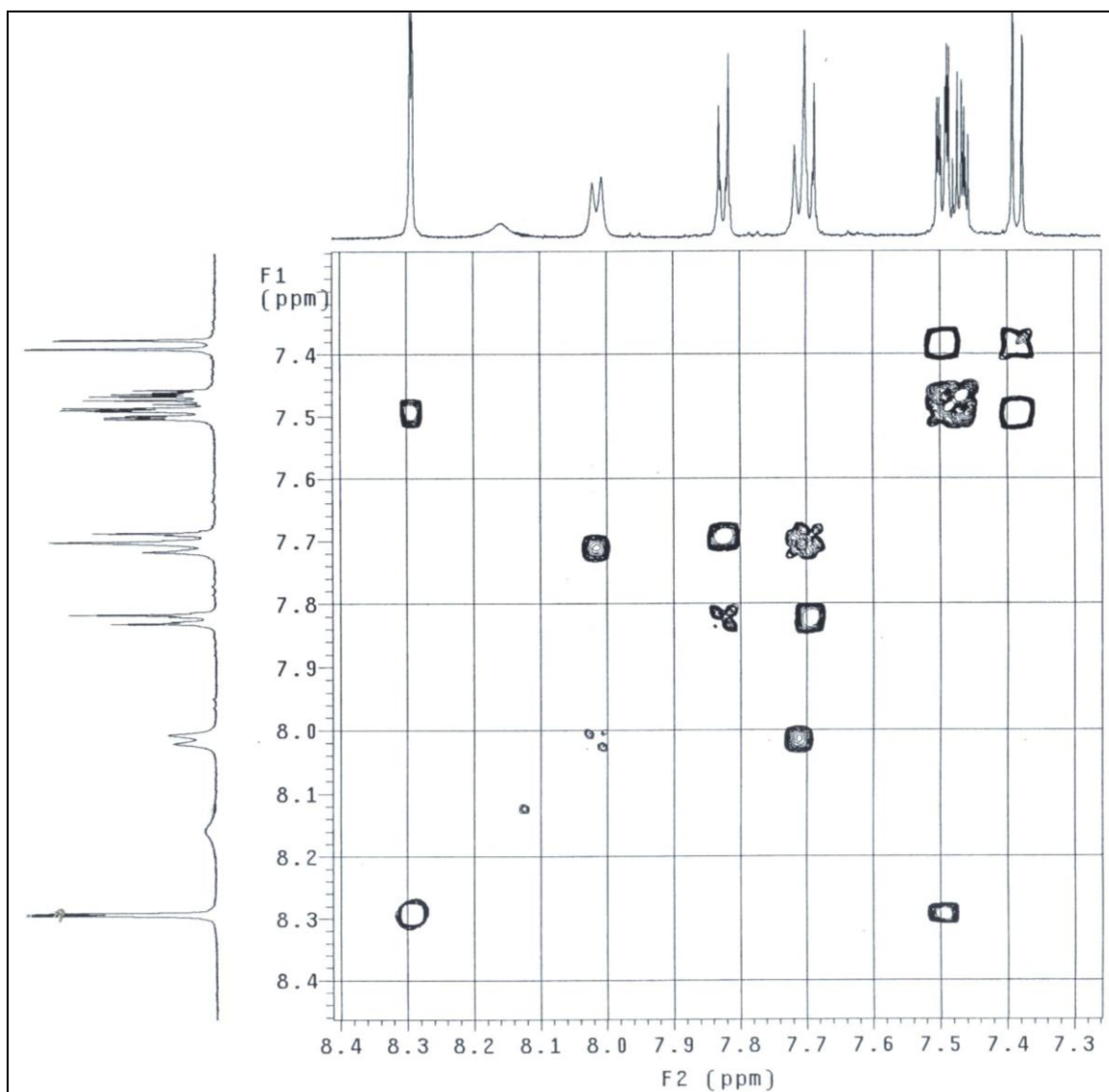


**Figure 2.17.** COSY spectrum of 2-cyano-3-(4-(2-(5-(2-(4-(3,6-di-*tert*-butyl-9*H*-carbazolyl)phenyl)ethynyl)-2,2'-bithiophenyl)ethynyl)phenyl)acrylic acid (**1**) in DMSO (600MHz) .

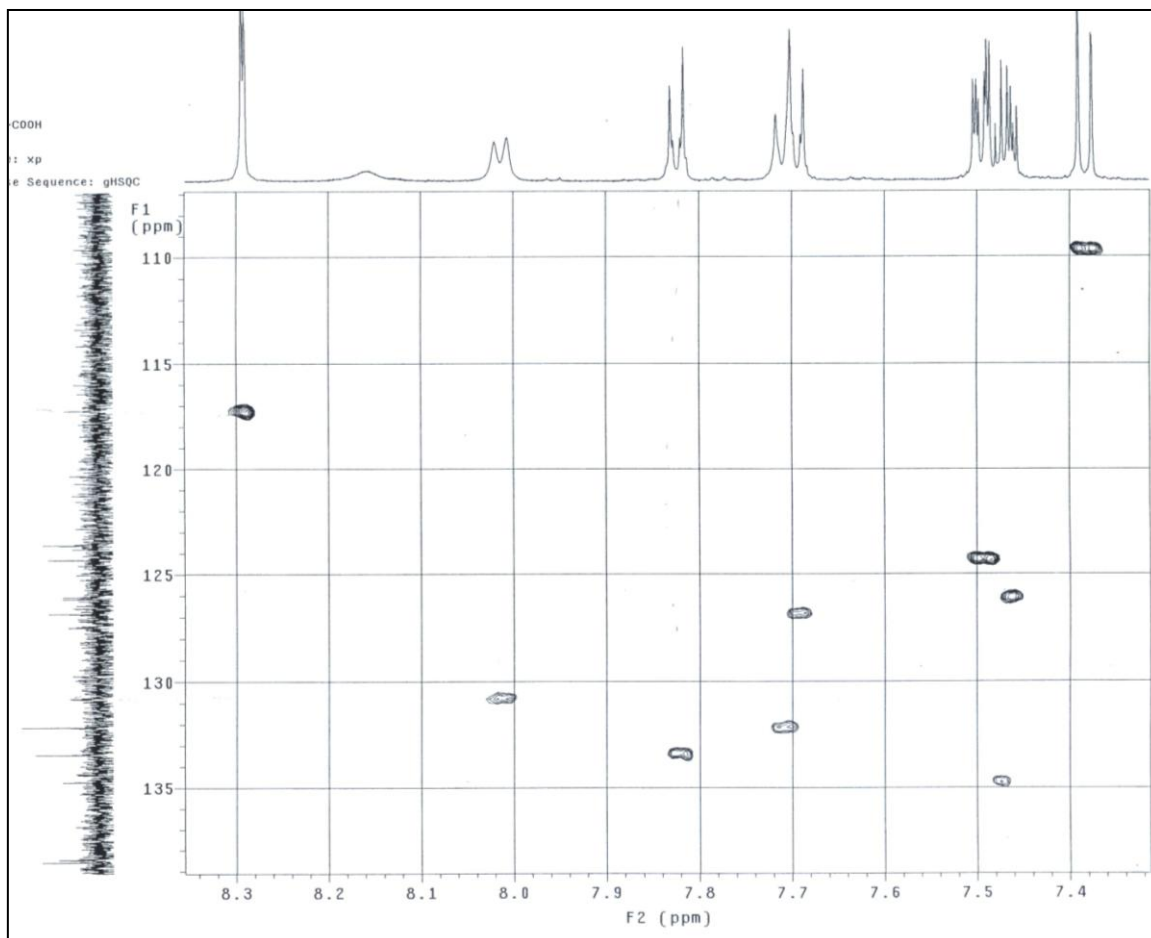


**Figure 2.18.** HSQC spectrum of 2-cyano-3-(4-(2-(5-(2-(4-(3,6-di-*tert*-butyl-9*H*-carbazolyl)phenyl)ethynyl)-2,2'-bithiophenyl)ethynyl)phenyl)acrylic acid (**1**) in DMSO (600MHz) .

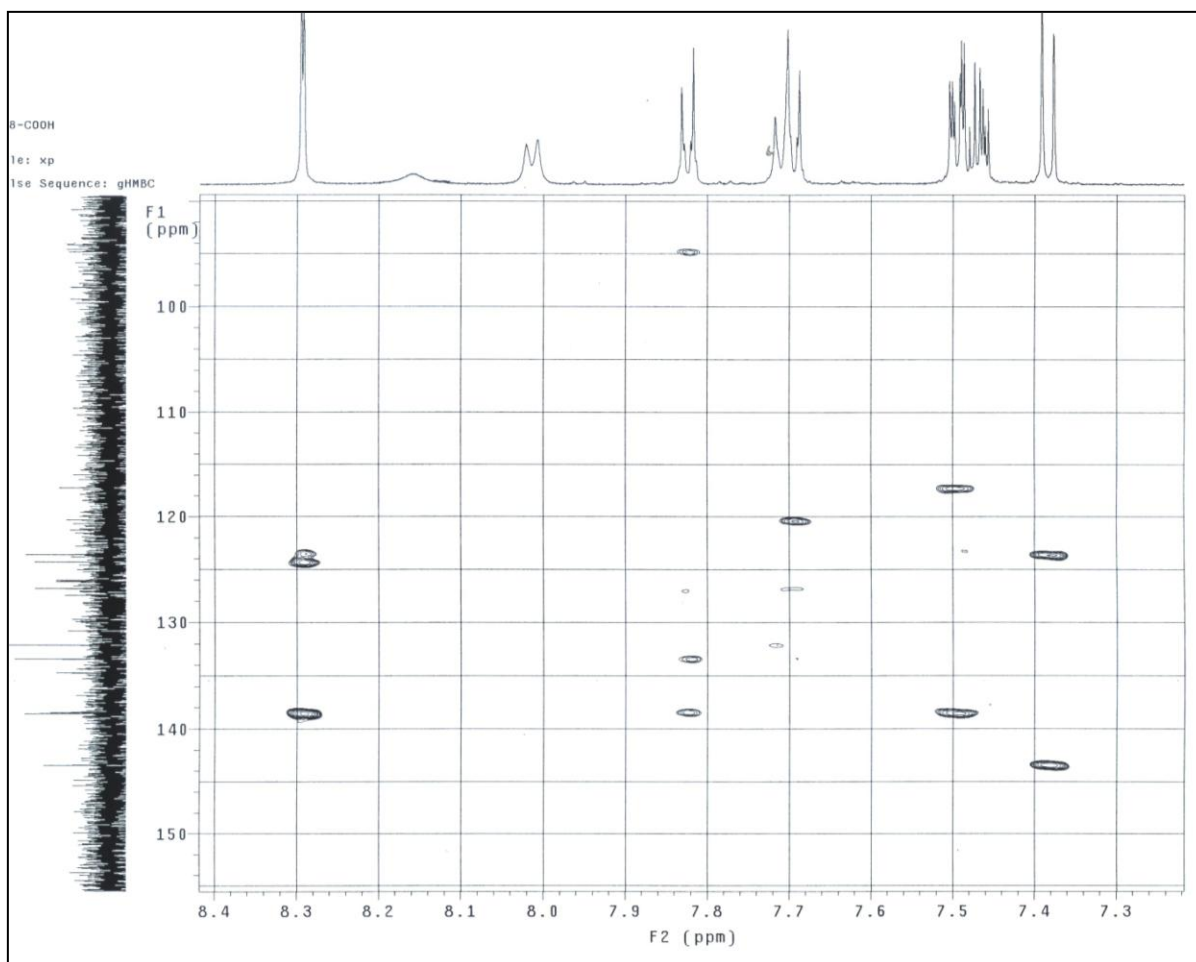


**Figure 2.19.** HMBC spectrum of 2-cyano-3-(4-(2-(5-(2-(4-(3,6-di-*tert*-butyl-9*H*-carbazolyl)phenyl)ethynyl)-2,2'-bithiophenyl)ethynyl)phenyl)acrylic acid (**1**) in DMSO (600MHz) .

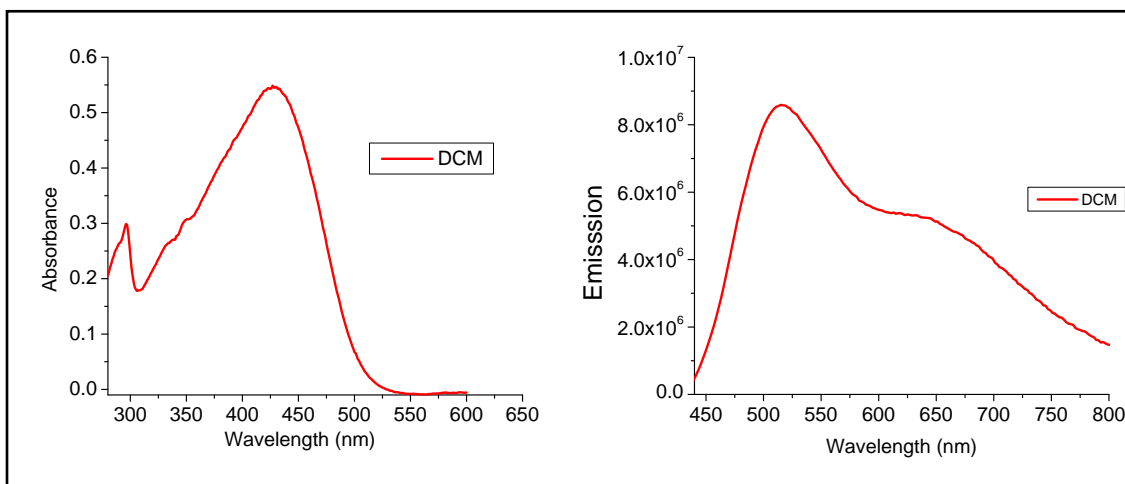


**Figure 2.20.** Absorbance and fluorescence spectra of **1**,  $\lambda_{\text{ex}} = 425$  nm.

**2.3.5. 2-((4-(2-(5-(2-(4-(3,6-di-*tert*-butyl-9H-carbazolyl)phenyl)ethynyl)-2,2'-bithiophenyl)ethynyl)phenyl)methylenyl)malononitrile (2)**

Compound **8** (50mg, 0.0745 mmol) , malononitrile (0.67 mmol) ,basic aluminum oxide (6.08 mmol), and dry toluene (20 ml) were placed in a 100 ml two necked round bottom flask. The mixture was refluxed under argon for 8 h and was filtered hot. The residue was washed several times with hot ethyl acetate. The filtrate was dried and the solid obtained was subjected to purification by prep-TLC (silica gel, DCM in hexane) and recrystallization (mixture of DCM and hexane) to obtain **2**.  $M^+(m/z) - 719$ . ( $M+2$  was observed)

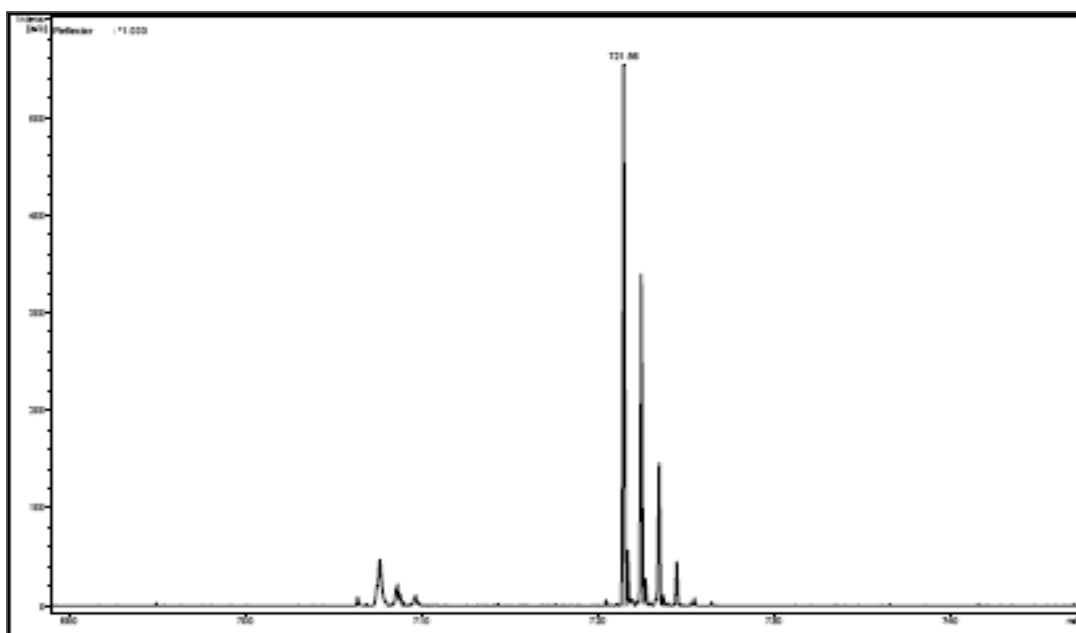


**Figure 2.21.** Mass spectrum of 2-((4-(2-(5-(2-(4-(3,6-di-*tert*-butyl-9H-carbazolyl)phenyl)ethynyl)-2,2'-bithiophenyl)ethynyl)phenyl)methylenyl)malononitrile (**2**).

## 2.4. Discussion and Conclusions

It is important to maintain an inert environment in the reaction vessel when synthesizing compound **6** and **8** because inactive palladium catalyst (Pd(II)) was used for the coupling reactions. If there is O<sub>2</sub> in the reaction vessel it will oxidize the active palladium (Pd (0)) which is converted by CuI and alkyne H of compound **5** and **7**. Since compound **5** and **7** were the one of the starting material for synthesizing compound **6** and **8** it is essential to add the exact amount of Pd (II) and CuI to the reaction mixture to optimize the reaction yield.

If compound **2** were converted into the dicarboxylic analog, a greater anchoring ability onto TiO<sub>2</sub> can be expected. Because of the time factor we couldn't complete the synthesis of compound **2**. MALDI showed the M+2 (721) ion peak instead of 719. It is acceptable because during the ionization process there is a possibility to attach excess hydrogen with the molecular ion. Since the reaction yield is very small, prep-TLC method was employed to purify the compound but NMR shows that the isolated product is not pure. Because of the time limitation, scale up process couldn't be started.

Compound **1** was successfully synthesized and completely characterized and it shows  $\lambda_{\text{max,ab}}$  at 425 nm in DCM. This is an encouraging evidence that compound **1** is a good candidate for making dye-sensitized solar cell.

We hope to make collaboration with another group who work with DSC in BGSU to test our compound for dye sensitized solar cells.

## 2.5. References

1. Tributsch, H. *Coord. Chem. Rev.* **2004**, *248*, 1511.
2. <http://en.wikipedia.org/wiki/Solar-cell>.
3. O'Regan, B.; Graetzel, M. *Nature*, **1991**, *353*, 737.
4. Hagfeldt, A.; Graetzel, M. *Chem. Rev.*, **1995**, *95*, 49.
5. Graetzel, M. *J. Photochem. Photobio.*, **2003**, *4*, 145.
6. [http://ec.europa.eu/energy/index\\_it.html](http://ec.europa.eu/energy/index_it.html).
7. Jayaweera, P. M.; Palayangoda, S. S.; Tennakone, K. *J. Photochem. Photobio.*, **2001**, *140*, 173.
8. Bauerle, P.; Wurthner, F.; Gotz, G.; Effenberger, F. *Synthesis*, **1993**, *11*, 1099.

## CHAPTER 3

### Chemical Enhanced Oil Recovery

#### 3.1. Introduction

In oil deposits (liquid hydrocarbon and gaseous products produced from wells drilled into underground petroleum-bearing reservoirs), oil is present in the cavities of porous reservoir rocks which are sealed toward the surface of the earth by impermeable top layers.<sup>1</sup> These cavities may be very fine cavities, capillaries, pores or the like. Fine pore necks may have a diameter of only approximately 1  $\mu\text{m}$ . As well as oil, including fractions of natural gas, a deposit comprises water with a salt content of roughly 5 to 20% by weight. The dissolved salt may include alkali metal salts; however, it also may be comprised of relatively high contents of alkaline earth metal ions, for example up to 5% by weight calcium ions and/or magnesium ions. Oil recovery can be categorized into three levels of extraction: primary, secondary and tertiary.<sup>1</sup>

In primary extraction, the deposit is drilled and then oil flows of its own accord through the borehole to the surface owing to the autogenous pressure of the deposit. The autogenous pressure can be caused by gases present in the deposit such as methane, ethane or propane. By means of primary extraction, (depending on the deposit type), it is usually possible to extract approximately 5 to 10% of the amount of oil present in the deposit. Thereafter the autogenous pressure is no longer sufficient for extraction.<sup>1</sup>

After primary extraction, secondary extraction is employed. In secondary extraction, in addition to so-called production bores, further boreholes which are called injection bores are drilled into the oil-bearing formation. Water is injected into the deposits through these injection bores in order to maintain the pressure. As a result of the injection of the water,

the oil is slowly forced through the cavities in the formation, proceeding from the injection bore, in the direction of the production bore.<sup>1</sup> However, this only works for as long as the cavities are completely filled with oil and the more viscous oil is pushed onward by the water, Figure 3.1.

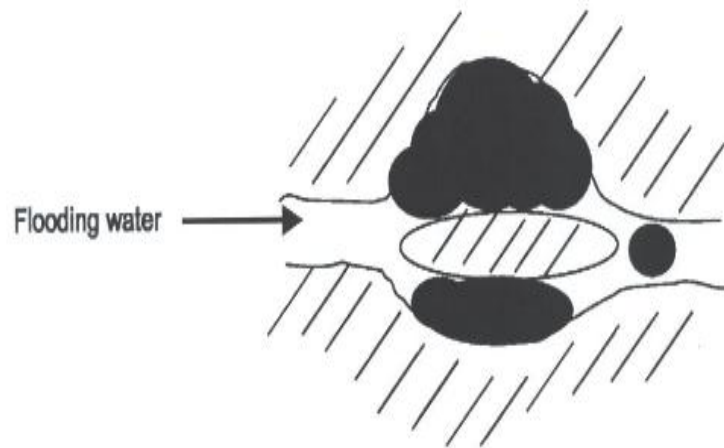


**Figure 3.1.** Water flooding through a cavity completely filled with oil.<sup>2</sup>

As soon as the mobile water breaks through the cavities, it flows on the path of least resistance, i.e. through the channel formed, and no longer pushes the oil onward. This situation is shown in Figure 3.2 owing to the different polarity of oil and water, a high interfacial tension arises between the two components. Therefore, these two components adopt the smallest contact area with respect to one another which results in a spherical oil droplet that no longer fits through the fine capillaries of the reservoir. At the end of the water flooding, the oil is thus trapped in the capillaries in isolated spherical droplets.

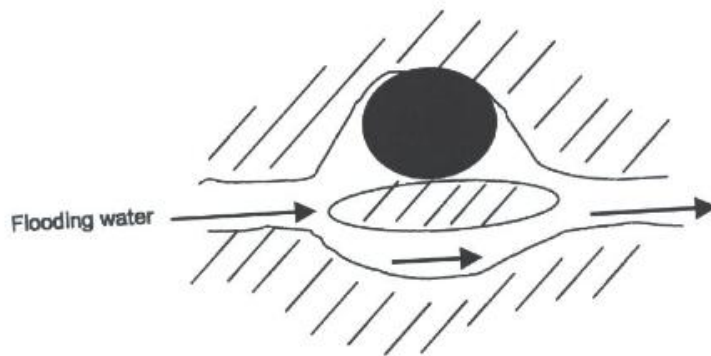


**Figure 3.2.** Oil in a capillary after water flooding.<sup>2</sup>

Generally 30 to 35% of the amount of oil present in the deposit can be extracted using primary and secondary extraction.

### **3.1.1. Tertiary Oil Recovery**

It is known that the oil yield can be enhanced further by tertiary oil extraction. Tertiary oil recovery also called Enhanced Oil Recovery (EOR) consists of injecting a displacing fluid into the injection wells in order to displace the oil and gas in a reservoir towards producing wells. There are many types of EOR techniques.<sup>1</sup> The most common types of EOR are thermal processes, where a hot invading phase, such as steam or hot water or a combustible gas, is injected, in order to increase the temperature of the oil and gas in the reservoir. This facilitates flow to the production wells by increasing the pressure and reducing the resistance to flow. Another EOR technique consists of injecting a phase that is miscible with the oil and gas into reservoir in order to eliminate the interfacial tension effects. The miscible phase can be a miscible hydrocarbon, CO<sub>2</sub> or inert gas.<sup>1</sup> Tertiary oil

extraction also includes methods in which suitable chemicals are used to aid for oil extraction. This is also called chemical flooding and a combination of Alkaline-Surfactant-Polymer (ASP) is injected into the reservoir. The Polymer is generally water soluble and it is used to improve the sweep efficiency of the invading fluids by changing the mobility ratio between the invading fluids (the ASP fluids) vs. the displaced fluid (of which the most important fluid is the oil). Most commonly used polymer in oil industry are partially hydrolyzed polyacrylamide and biopolymers (such as xanthan gum).<sup>3</sup> The surfactant is present to change the wettability of the formation rock, if necessary, and to reduce the interfacial tension.<sup>1</sup>

It is desired that with surfactant flooding the oil droplets subsequently combine to form a continuous oil bank. This is shown schematically in Figure 3.3.



**Figure 3.3.** Surfactant flooding through a cavity with filled with oil.<sup>2</sup>

The oil bank is important for two reasons: firstly, as the continuous oil bank advances through new porous rock, the oil droplets present there can merge with the bank.

Secondly, the combination of the oil droplets to form an oil bank significantly reduces the oil-water interface, and the surfactant which is no longer required is thus released. The released surfactant can mobilize the remaining oil droplets in the formation. This is

shown schematically in Figure 3.4. An ultra-low interfacial tension between the water phase and oil phase is also required to combine the oil droplets to an oil bank and to incorporate new oil droplets into the it. Otherwise individual oil droplets remain or are not incorporated into the oil bank. This reduces the efficiency of surfactant flooding.

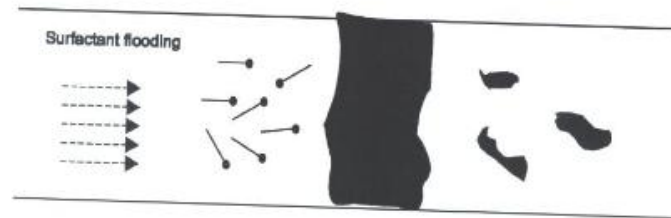


**Figure 3.4.** Surfactant flooding forming oil bank in the cavity.<sup>2</sup>

Another key oil recovery problem in an oil-wet reservoir is overcoming the surface tension forces that bind the oil to the rock. In a water-wet reservoir, surface tension forces act to create droplets of oil, which can block pore passages as the droplets resist movement due to the greater surface area associated with squeezing through the passages. These surface tension forces are the primary reasons are to why the oil reservoir becomes increasingly impermeable to oil, relative to water, when the water saturation increases.<sup>4</sup> Surfactant use for oil recovery is not a recent development in petroleum technology. De Groot obtained a patent in 1929 claiming water-soluble surfactants can aid EOR.<sup>5</sup> In 1962, Gogarty and Olson of Marathon Oil Co. filed for a patent, based on their field trial where they used petroleum sulfonates along with a chemical slug containing hydrocarbons, water, electrolyte and co-surfactants.<sup>6</sup> Since then, thousands of research papers, patents, and proceedings have been published on surfactant flooding EOR. In addition, numerous

field operations have been going on around the world. The success of surfactant flooding EOR depends on many factors: the cost and effectiveness of the surfactant formulation, availability of chemicals, environmental impact, and oil prices in the market.

A three-stage procedure has been developed at The University of Texas at Austin for the selection and screening of surfactants for EOR applications.<sup>7</sup> First, a preliminary list of surfactants is assembled based upon the surfactant structure and interfacial activity, knowledge and experience, and the specific physicochemical conditions of the targeted reservoir. Co-surfactants, co-solvents, alkali, and polymer may be added to optimize the performance of the surfactant at this stage. Favorable structural attributes of the surfactant include branched hydrophobes which reduce the formation of viscous phases, and the addition of ethylene oxide and/or propylene oxide units, which can be used to tailor the surfactant to a broader range of conditions.

Next, the candidate surfactants are screened in phase behavior experiments that measure micellar solubilization of test oils over a range of salinity conditions, as described by Healy et al. (1976).<sup>8</sup> Interfacial Tension (IFT) can be calculated from these solubilization values as developed by Huh (1979) and discussed further in 3.1.2.<sup>9</sup> Other factors such as viscosity, equilibration time, and aqueous phase solubility are also used to evaluate candidate surfactant formulations.

The third and final phase of testing involves oil recovery experiments in outcrops and reservoir cores. These are flow experiments using consolidated rock cores or small core plugs which are assembled in series.

### 3.1.2. Background of phase behavior screening

The formation of distinct, thermodynamically stable phases when surfactant, oil and brine are mixed was first described by Winsor (1954).<sup>10</sup> Such phases are fundamentally different from macroemulsions, which are thermodynamically unstable. The surfactant-rich phase has come to be referred to as “microemulsion,” and this terminology will be used here to describe certain stable mixtures of surfactant, oil and brine. The term “macroemulsion” will be used to describe true emulsions, which are thermodynamically unstable though they may be kinetically quite stable when they have a high viscosity.

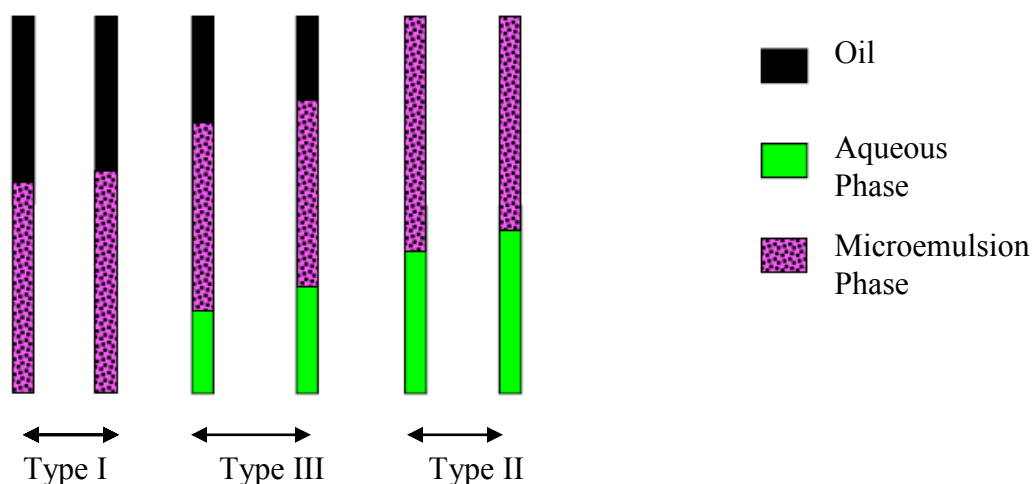


**Figure 3.5.** Winsor surfactant phase behavior categories.

Microemulsion phase behavior is described as Winsor type I, type II, and type III, Figure 3.5.<sup>7</sup> A transition in phase behavior can be caused by changing variables such as salinity, temperature, surfactant structure, or equivalent alkane carbon number (EACN)

of the oil. At low salinity, type I or oil-in-water microemulsions occur, and there are characterized by coexistence with an excess brine phase. At very high salinity, type II or water-in-oil microemulsions are formed, which are characterized by coexistence with an excess oil phase. A narrow intermediate range exists between the type I and type II regions that is called the type III region in which bilamellar oil and water microemulsions are formed as a middle phase that coexists with both excess oil and excess water phases. The salinities at which the transition occurs between types I and type III behavior is referred to as the lower critical salinity, and the salinity of the transition between type III and type II is referred to as the upper critical salinity. The salinity at which equal volumes of oil and water are solubilized in the microemulsion is defined as the optimal salinity. Optimal salinity has also been defined as the salinity at which the interfacial tension between the microemulsion and water equals that between the microemulsion and oil and is typically the same as the salinity for equal solubilization. The optimal salinity is approximately at the midpoint between the lower critical salinity and the upper critical salinity.

In surfactant flooding, the surfactant should generally form a middle-phase microemulsion (Winsor type III) with the water phase and oil phase.<sup>7</sup> Figures 3.6 and 3.7 shows the phase behavior tubes with a salinity gradient where a middle-phase microemulsion is observed. A Winsor type III microemulsion is a thermodynamically stable, liquid mixture of water, oil, and surfactant which has a very low interfacial tension and usually possesses a low viscosity. The microemulsion is in equilibrium with both excess water and excess oil phases. A low viscosity is desirable to transport the microemulsion in the oil formation. At an excessively high viscosity of the phase to be

transported, a very high pressure would be necessary in the course of polymer flooding. In addition to being expensive there is a risk that this pressure might blast undesirably new cavities in the oil reservoir. In addition, excessively high viscosities hinder the formation of a continuous oil bank in combining the mobilized oil.

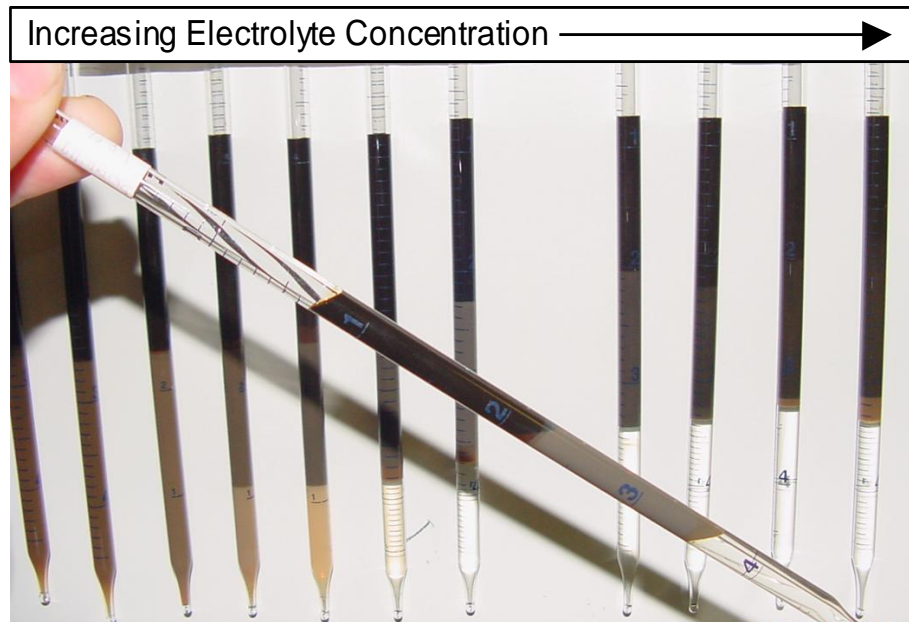


**Figure 3.6.** Microemulsion phase behavior as a function of salinity with one pipette tilted.<sup>7</sup>



**Figure 3.7.** Pipette from a microemulsion phase behavior salinity scan experiment being inverted.<sup>7</sup>

Surfactants have been investigated for use in enhanced oil recovery for over 40 years.

Early work focused on the injection of microemulsions containing high concentrations of surfactant, co-solvent, and oil,<sup>11</sup> which while technically successful was not economically viable due to the high chemical costs and low oil price at the time. Later work focused on reducing the amount of chemicals required and emphasized low concentration aqueous surfactant solutions with polymer added for mobility control rather than the injection of a microemulsion. Austad and Milter provide an overview of surfactant flooding developments up to 2000 including the development of EOR surfactants with EO and PO groups.<sup>12</sup> However, alkaline-surfactant-polymer flooding was not reviewed even though that has been a major emphasis since about 1984.<sup>13</sup>

Another trend in this field involves a more empirical approach, whereby the chemicals (which may include one or more surfactants, co-solvent, alkali, etc.) that exhibit the

lowest IFT towards the investigated crude oil, reservoir temperature, and often the formation salinity is taken as optimum, and a surfactant-polymer slug is injected at these conditions. Major weaknesses of this approach include lack of robustness to measurement error and local heterogeneities and susceptibility of surfactant to adsorption. Given the wealth of information accumulated over the last four decades, a more viable design and methodical screening process as can now be developed.

Aoudia et al. present several key relationships between surfactant structure, EACN, temperature, optimum salinity, and solubilization ratios of surfactant-brine-oil mixtures for surfactants with different propoxy numbers.<sup>14</sup>

Healy and Reed developed an empirical correlation between the solubilization ratios and the interfacial tension between the microemulsion and each excess phase.<sup>15</sup> Huh derived a theoretical relationship between the solubilization ratio and IFT.<sup>9</sup> A simplified form of his theory predicts the IFT ( $\gamma$ ) is inversely proportional to the square of the solubilization ratio ( $\sigma$ ):

$$\gamma = \frac{C}{\sigma^2} \quad (1)$$

where C is approximately 0.3 dynes/cm and the solubilization ratio ( $\sigma$ ) is defined as the volume of oil or water solubilized divided by the volume of surfactant on a 100% active basis. The solubilization ratio is much more easily and accurately measured over time than IFT and therefore is a useful surrogate for measuring IFT directly.

Because of the high IFT between water and oil half of the original oil in place remains in the reservoir after water flooding. This is due to trapping of oil droplets by capillary forces. The ratio of viscous forces, which favor oil mobilization, to capillary forces, which favor oil trapping, is quantified by the capillary number ( $N_c$ ). The relationship

between capillary number and IFT shows is in equation 2 where  $\Delta P/L$  is the pressure gradient along the capillary and  $\sigma$  is the IFT between displaced and displacing fluids and  $k$  is the permeability.<sup>16</sup>

$$N_c = \frac{k \cdot \Delta P}{L \sigma} \quad (2)$$

Typical water flood capillary numbers are  $10^{-7}$ . Taber reported that an increase in capillary number to between  $10^{-4}$  and  $10^{-3}$  is necessary to improve oil recovery<sup>16</sup>. Figure 3.8 illustrates the relationship between capillary number and residual oil saturation. According to above equation when the IFT is lower, the capillary number will increase. Achieving ultra-low IFT on the order of  $10^{-3}$  dynes/cm is necessary to mobilize the residual oil in reservoir rocks and to reduce the oil saturation towards zero under typical pressure gradients in oil reservoirs.<sup>16</sup> However, additional conditions must be satisfied for surfactant-polymer flooding to be both efficient and practical under reservoir conditions. In order to transport surfactant solutions at low pressure gradients ( $\sim 1$  psi/ft) encountered in typical oil reservoirs, highly viscous phases must be avoided. Macroemulsions, gels, and liquid crystals are often viscous and should be avoided because they result in high surfactant retention and ultimately poor oil recovery. Viscous phases tend to occur when surfactant molecules form ordered structures. These structures can be minimized by several methods: the addition of co-solvent, the use of co-surfactants with differing structure, or by using surfactants with branched hydrophobes. This last method is preferable because co-surfactants and co-solvents increase cost and may decrease solubilization as well.

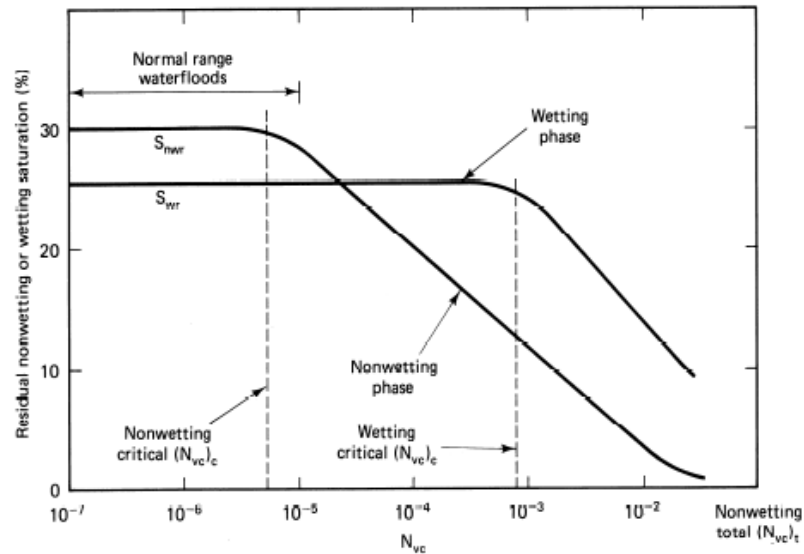


**Figure 3.8.** Schematic capillary desaturation curve.<sup>17</sup>

In addition to the use of hydrophobe branching, researchers including Aoudia et al.<sup>14</sup> and Salager et al.<sup>18</sup> have described the beneficial effects of including propylene oxide (PO) and ethylene oxide (EO) units in sulfate surfactant molecules. These units can be added between the hydrophobe and hydrophile in order to allow the groups to extend further into the aqueous and oil phases, respectively. The net effect is increased solubilization, as well as a broader region of low IFT due to the interfacial affinity of the PO and EO groups. An additional benefit is increased calcium tolerance.

Zhang et al. found that sodium carbonate reduces the adsorption of anionic surfactants on carbonate minerals.<sup>19</sup> The use of sodium carbonate makes chemical flooding of carbonates less expensive and thus more profitable at current crude oil prices. Previous work by Nelson et al. has shown the benefits of reduced chemical adsorption on sandstones with the use of sodium carbonate, but most workers have assumed that either

cationic or non-ionic surfactants would be preferred for carbonates, so the use of anionic surfactants is an entirely new development that now seems feasible when sodium carbonate is used to raise the pH.<sup>13</sup>

Adkins et. al. discovered that dimerized alcohols (Guerbet alcohols) with ethoxy and propoxy sulfate can be used for lowering IFT and lower the microemulsion viscosity even under high temperature and high salinity conditions.<sup>20</sup>

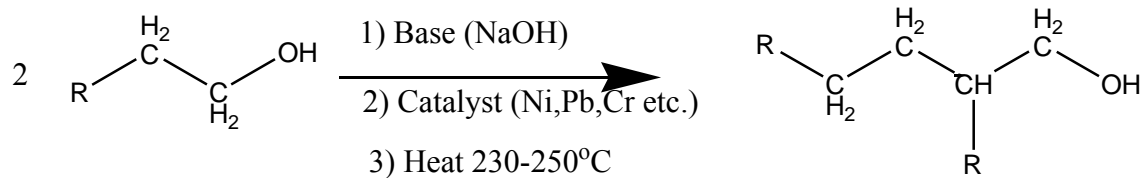
### **3.1.3. Guerbet Alkoxy Sulfate Surfactants**

Oil reservoirs containing heavy crude oil, high-temperature, and/or high-salinities provide many challenges for chemical EOR. When the equivalent alkane carbon number of the crude oil is high, surfactants with very large hydrophobes and branched structures are required to obtain ultra-low interfacial tensions and low microemulsion viscosities.<sup>21</sup> However, the cost of these very large hydrophobe surfactants can be quite high.

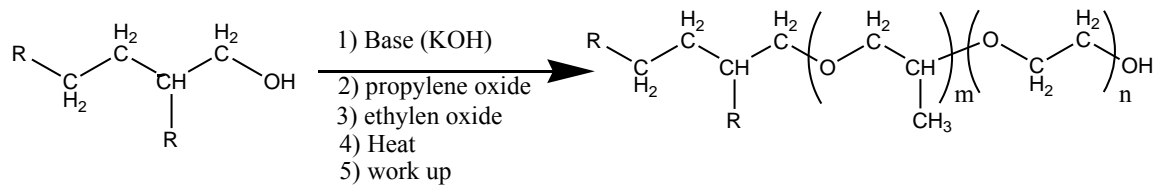
The Guerbet reaction dimerizes a linear alcohol using base catalysis at high temperatures (for example 230 °C) to produce near mid-point branching (Figure. 3.9).<sup>22</sup> The Guerbet alcohols (GA) are considered the “gold” standard for large, branched alcohols which are low melting liquids. Very large hydrophobe structures can be produced from smaller linear alcohols using the Guerbet reaction. For example, a C<sub>32</sub> GA can be produced from a C<sub>16</sub> alcohol. These Guerbet alcohols (GA) can then be used in the production of corresponding alkoxy sulfate surfactants. These anionic surfactants can be produced by adding propylene oxide (PO) and ethylene oxide (EO) units to the GA, followed by

sulfation (Figure 3.9 and 4.1).<sup>23</sup> By varying the amount of PO and EO in the Guerbet surfactants, they can be tailored to fit specific EOR needs.

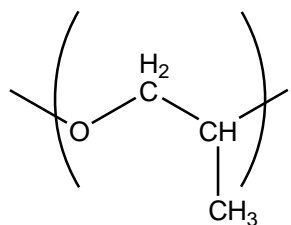
Guerbet alcohols tend to be more expensive than other alcohols when produced in high purity for various industrial applications.<sup>24</sup> The high cost is mainly due to driving the reaction to completion and/or stripping-off of the unreacted monomer alcohol to produce high purity. However, inexpensive Guerbet alcohols (GA) can be prepared by aiming for less than quantitative conversion during the alcohol dimerization process. The resultant blend of 85-95% GA and 5-15% monomer alcohol is subsequently used in the alkoxylation process to add propylene oxide and/or ethylene oxide, followed by sulfation. Such mixtures are both less expensive and more effective when made into anionic surfactants for enhanced oil recovery than higher purity GA products that require more reactor time and higher cost to manufacture. The unreacted alcohol monomer subsequently ends up as a co-surfactant during the surfactant manufacturing process with the mixture of surfactants being as effective as the pure surfactant. When higher purity GA are used to produce the alkoxy sulfates, the final surfactant molecules are still of reasonable cost due to the high molecular weight of the sulfate surfactant. For example, in Guerbet C32-7PO-10EO sulfate the GA is only 38% of the entire surfactant molecule based on weight. Through the use of this new Guerbet process, these surfactants can be manufactured at low cost when made as sulfates as opposed to sulfonates.



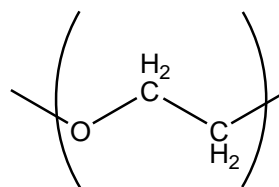
R=Alkyl group



R=Alkyl group



PO = propoxy group



EO = ethoxy group

**Figure 3.9.** Synthesis scheme for Guerbet alkoxy alcohol with PO and EO groups.

## CHAPTER 4

### Experimental Methods Results and Discussion

#### 4.1. Surfactant and Materials

The Guerbet alkoxyates, including  $C_{20}H_{41}-7PO-OH(C20-7PO-OH)$ ,  $C_{20}H_{41}-7PO-6EO-OH(C20-7PO-6EO-OH)$ ,  $C_{20}H_{41}-7PO-10EO-OH(C20-7PO-10EO-OH)$ ,  $C_{20}H_{41}-7PO-14EO-OH(C20-7PO-14EO-OH)$ ,  $C_{28}H_{57}-7PO-2EO-OH(C28-7PO-2EO-OH)$ ,  $C_{28}H_{57}-7PO-6EO-OH(C28-7PO-6EO-OH)$ ,  $C_{32}H_{65}-7PO-6EO-OH(C32-7PO-6EO-OH)$ ,  $C_{32}H_{65}-7PO-10EO-OH(C32-7PO-10EO-OH)$ ,  $C_{32}H_{65}-7PO-14EO-OH(C32-7PO-14EO-OH)$ , were obtained from Harcros Chemicals, Inc. and were sulfated via standard sulfamic acid sulfation as being practiced commercially.

The surfactant  $C_{20-24}$  IOS (internal olefin sulfonates) which contain mixture of hydroxyalkanesulfonate (HAS) and alkenesulfonate (IOS), was obtained from Stepan Company and used as received (structure in Figure 4.1)

The salts used to make the brine (for example sodium chloride, sodium carbonate, and sodium sulfate) are obtained from Fisher Chemical and used as received. The co-solvent triethyleneglycolmonobutylether (TEGBE) was purchased from Aldrich Chemicals and used as received. The polymer AN 125 was obtained from SNF.

The sodium dihexyl sulfosuccinate (or sodium di(1,3, dimethylbutyl)sulfosuccinate or Aerosol MA-80I) was obtained from Cytec Industries Inc. and was used as received. The co-solvents TDA-30 ( $C_{13}H_{27}(OCH_2CH_2)_{30}OH$ ) and TDA-12 ( $C_{13}H_{27}(OCH_2CH_2)_{12}OH$ ) were obtained from Sasol North America Inc. and used as received. Sulfamic acid was purchased from MP Biomedicals and used as received.

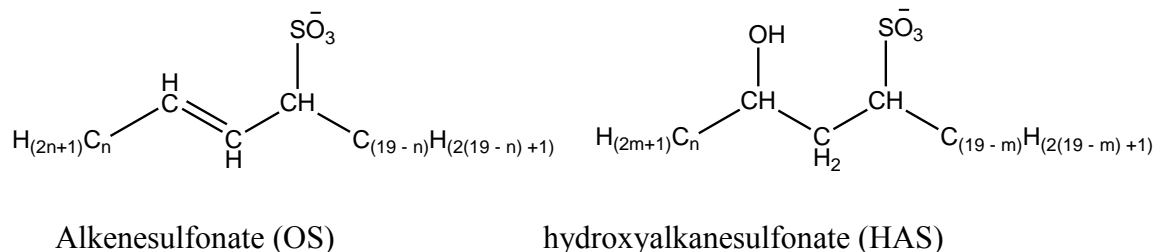


**Figure 4.1.** Structures of two sulfonates in  $\text{C}_{20-24}$  IOS.

## 4.2 Experimental Procedures

### 4.2.1. Sulfation of Guerbet alkoxy alcohols.

The sulfation of an alkoxy alcohols can be carried out using a variety of sulfation reagents, most commonly  $\text{SO}_3$  (sulfur trioxide) and  $\text{HSO}_3\text{Cl}$  (chlorosulfonic acid).<sup>24</sup> However in this case less aggressive sulfamic acid was used as the sulfation agent which is also commonly use in industry. The procedure for sulfation is as follows: 1 mole equivalent of Guerbet alkoxy alcohol (22.85g of C32-7PO-6EO-OH, 1136 g/mol) was added to a two necked flask with a stir bar and heated until melted. Then 1.1 mole equivalents of sulfamic acid (2.15g of 97.1 active sulfamic acid) were added to the flask (i.e. the mole ratio of GA to sulfamic acid is 1:1.1). The sulfation reaction then proceeded 2 to 3 days at 80 °C under a nitrogen environment (Figure 4.2). The reaction was monitored using  $^{13}\text{C}$  NMR. After that a dilution of 10% surfactant solution was made using alkaline DI water using  $\text{Na}_2\text{CO}_3$  to maintain a pH at 8-9.  $^{13}\text{C}$  NMRs of C32-7PO-6EO-OH and the corresponding sulfate are attached in the Appendix (Figure A6 and A7)

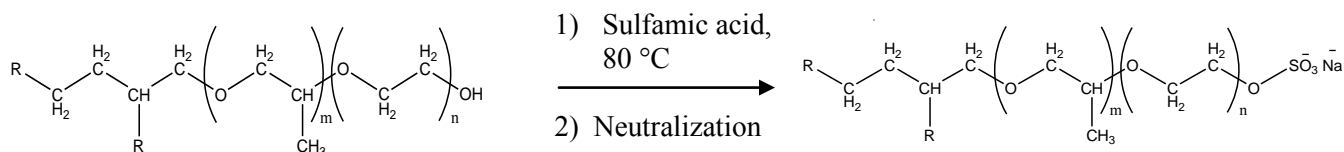


**Figure.4.2.** Sulfation reaction of Guerbet alkoxy alcohol.

#### 4.2.2. Aqueous Solubility Experiments

The aqueous solubility of alkoxy sulfate surfactants at 25 and 85 °C are tested by studying surfactant solutions with polymer because the solutions must be clear both at the injection temperature and the reservoir temperature. In the visual observation studies, the surfactant-polymer mixtures are checked for turbidity and phase separation of the surfactant from the aqueous solution. A 4x concentrated surfactant stock solution is made consisting of the alkoxy sulfate surfactant in de-ionized (DI) water (18 ohm) or brine at a slightly basic pH. The quantity of surfactant in the concentrated stock is calculated based on the activity and measured by weight percent of total solution. An alkali stock solution is also made in a plastic container. A polymer stock solution of 5000 ppm polymer (SNF experimental polymer) is also used. The stock solutions are used to make 10 ml samples (in 20 mL glass vials, Fisher Scientific) with the desired surfactant concentration, polymer concentration, and gradient in the alkali (sodium carbonate) concentrate. Components are added volumetrically into the vials using an Eppendorf Repeater Plus or similar pipetting instrument with removable plastic tips. The polymer is added first generally at a volume of 2.5 ml, followed by DI water, brine, alkali, and finally surfactant. The samples are mixed on a vortex mixer (Scientific Industries). Visual observations are recorded at room temperature. Next, the samples are placed in racks in convection ovens at the elevated temperature. Visual observations are taken once the temperature of the samples has equilibrated with the oven. The sample with the highest alkali concentration that remains clear with no phase separation or precipitation is recorded as the aqueous solubility limit.

### 4.2.3. Phase Behavior Experiments

Surfactant formulations are tested in the presence of oil and brine to find and measure the middle-phase microemulsion. The chemicals being tested are first mixed in a concentrated stock solution (typically 4X) that usually consist of a primary surfactant, co-solvent and/or co-surfactant along with de-ionized water (18 ohm) or brine at a basic pH (9-11). The weight of chemical added is calculated based on the activity of the chemicals and measured by weight percent of total solution.<sup>7, 25, 26</sup> Standard 5 ml borosilicate pipettes with 0.1 ml markings are used to create phase behavior scans as well as run dilution experiments with aqueous solutions. Phase behavior components (including brine, alkali, DI water, and surfactant stock) are added volumetrically into the 5 ml pipettes using a repeater or similar pipetting instrument. Once the components are added to the pipettes, sufficient time is allotted to allow all the fluid to drain down the sides. Then initial aqueous fluid levels are recorded before the addition of the crude oil. The pipettes are blanketed with Argon gas to replace oxygen to prevent the ignition of any volatile gas present by the flame sealing procedure. The tubes are then sealed with the propane-oxygen torch to prevent loss of additional volatiles when placed in the oven. Pipettes are arranged on the racks to coincide with the change in the scan variable (such as salinity in terms of brine, alkali, co-solvent, or oil concentration). The typical phase behavior scan consisted of 10-20 pipettes, each pipette being recognized as a data point in the series. Once the phase behavior scan is given sufficient time to reach reservoir temperature (15-60 minutes), the pipettes are inverted several times for mixing. Tubes are observed for low tensions upon mixing by looking to determine equilibration time and surfactant performance. Initial experiments use about 1-3% active surfactant so that the volume of

the middle microemulsion phase is large enough for accurate interfacial measurements. Almost all of the phase behavior experiments are initially created with a water oil ratio (WOR) of 1, which involved mixing 2 ml of the aqueous phase with 2 ml of the crude oil or hydrocarbon. Different WOR experiments are mixed accordingly. WOR of 1-9 are used with the higher WOR experiments being more important for core flood and reservoir purposes. Multiple WOR values are studied in an “oil scan” which is typically conducted for high performing surfactant formulations.

The oil and water solubilization ratios are calculated from interface measurements taken from the phase behavior pipettes. These interface readings are recorded over time as the solutions approach equilibrium and the volume of any macroemulsion that initially form decrease or disappear. The oil solubilization ratio is defined as the volume of oil solubilized in the aqueous or middle phase divided by the volume of surfactant in that phase. All the surfactant is presumed to be in the emulsion phase. The volume of oil solubilized is found by reading the change between the initial aqueous level and the excess oil (top) interface level. Similarly, the water solubilization ratio is defined as the volume of water solubilized divided by the volume of surfactant in the oil or microemulsion phase (assumed to be the total surfactant volume). The volume of water solubilized is found by reading the change between the initial aqueous level and the excess water (bottom) interface level. The optimum solubilization ratio occurs where the oil and water solubilization ratios are equal as determined by drawing oil and water solubilization ratio curves from the specific data points (one per pipette).<sup>7</sup> Table 4.1 and 4.2 show the properties of the crude oil and composition of the reservoir Synthetic brine

(SB) and Synthetic soft brine (SSB) which were used for the experiments and Table 4.3 shows the surfactant formulations which were investigated for the phase behavior studies.

**Table 4.1** Description of Crude Oil

Oil Label	Temperature	Viscosity (cP)	Comments
#1	85°C	6.6	High paraffin content, solid at room temperature

**Table 4.2** Composition of Synthetic Brine (SB) and Synthetic Soften Brine (SSB)

Concentration (mg/L)	SB	SSB
Na <sup>+</sup>	900	932
Ca <sup>+</sup>	20	0
Mg <sup>+2</sup>	5	0
Fe <sup>+3</sup>	0	0
Ba <sup>+2</sup>	0	0
K <sup>+</sup>	15	15
Sr <sup>+2</sup>	0	0
Cl <sup>-</sup>	800	800
SO <sub>4</sub> <sup>-2</sup>	18	18
CO <sub>3</sub> <sup>-2</sup>	0	0
HCO <sub>3</sub> <sup>-</sup>	1100	1100
TDS	2858	2865

**Table 4.3** Formulations used for Phase Behavior Screening

Experiment Number	Primary Surfactant (P.S.)	Weight % of P.S.	Secondary Surfactant (S.S.)	Weight % of S.S.	Co-solvent	Weight % of Co-solvent
1	Guerbet C20-7PO-Sulfate	1	–	–	TEGBE	0.5
2	Guerbet C20-7PO-Sulfate	0.5	C <sub>20-24</sub> IOS	0.5	TEGBE	0.5
3	Guerbet C20-7PO-6EO-Sulfate	1	–	–	TEGBE	0.5
4	Guerbet C20-7PO-6E-Sulfate	1	C <sub>20-24</sub> IOS)	0.5	TEGBE	0.5
5	Guerbet C20-7PO-17E-Sulfate	1	–	–	TEGBE	0.5
6	Guerbet C28-7PO-2EO-Sulfate	0.5	C <sub>20-24</sub> IOS)	0.5	TEGBE	0.5
7	Guerbet C28-7PO-2EO-Sulfate	0.5	C <sub>20-24</sub> IOS)	0.75	TEGBE	0.5
8	Guerbet C28-7PO-2EO-Sulfate	0.5	Guerbet C20-7PO-Sulfate	0.5	TEGBE	0.5
9	Guerbet C28-7PO-2EO-Sulfate	0.5	Guerbet C20-2EO-Sulfate	0.5	TEGBE	0.5
10	Guerbet C28-7PO-2EO-Sulfate	0.5	Guerbet C20-6EO-Sulfate	0.5	TEGBE	0.5
11	Guerbet C28-7PO-2EO-Sulfate	0.3	Guerbet C20-6EO-Sulfate	0.3	TDA 30	0.3
12	Guerbet C28-7PO-2EO-Sulfate	0.3	Guerbet C20-6EO-Sulfate	0.3	TDA 12	0.3
13	Guerbet C32-7PO-6EO-Sulfate	0.3	Guerbet C20-6EO-Sulfate	0.3	TDA 30	0.1
14	Guerbet C32-7PO-6EO-Sulfate	0.3	C <sub>20-24</sub> IOS	0.3	TDA 30	0.2
15	Guerbet C32-7PO-6EO-Sulfate	0.3	C <sub>20-24</sub> IOS	0.3	TDA 30	0.1
16	Guerbet C32-7PO-6EO-Sulfate	0.3	C <sub>20-24</sub> IOS	0.3	TDA 30	0.1
17	Guerbet C32-7PO-6EO-Sulfate	0.3	C <sub>20-24</sub> IOS	0.3	–	–
18	Guerbet C32-7PO-6EO-Sulfate	0.45	C <sub>20-24</sub> IOS	0.15	–	–
19	Guerbet C32-7PO-6EO-Sulfate	0.4	C <sub>20-24</sub> IOS	0.2	–	–

20	Guerbet C32-7PO-6EO-Sulfate	0.42	C <sub>20-24</sub> IOS	0.18	–	–
21	Guerbet C32-7PO-6EO-Sulfate	0.5	Guerbet C20-6EO-sulfate	0.5	–	–
22	Guerbet C32-7PO-6EO-Sulfate	0.5	C <sub>20-24</sub> IOS	0.5	TEGBE	0.5
23	Guerbet C32-7PO-6EO-Sulfate	0.5	C <sub>20-24</sub> IOS	0.5	TEGBE, MA-80-I	0.5, 0.4
24	Guerbet C32-7PO-6EO-Sulfate	0.25	C <sub>20-24</sub> IOS	0.25	TEGBE, MA-80-I	0.25, 0.4
25	Guerbet C32-7PO-10EO-Sulfate	0.25	C <sub>20-24</sub> IOS	0.25	TEGBE, MA-80-I	0.25, 0.4

#### 4.2.4. ASP Core Flood Procedure

Core flood experiments test the surfactant formulation in a rock core in simulated reservoir conditions. The purpose of presenting these experiments is to validate the surfactant formulations obtained by phase behavior and aqueous solubility experiments.

Core flood experiment #1 with the crude oil (Table 4.1) was conducted on Bentheimer sandstone at 85 °C with a length of 28.575 cm and a diameter of 5.03 cm (Table 4.4 presents the core properties). The properties of the Bentheimer core for Core flood #2 are presented in Table 4.5.

The procedure listed below was used on each core to complete the core flood experiments. 5-minute epoxy was used to affix the two end pieces to the core. The core was then placed inside a homemade rectangular Teflon mold and cast in slow-setting epoxy with a hardener to epoxy ratio of 1:2 at 55 °C. Differential pressure transducers are used to measure the pressure drop across several sections of the core during flooding as shown in Figure 4.3. The absolute pressure of the core is also measured. The pressure readings are recorded by computer during flooding. Effluent from the core is captured in glass test tubes which are changed every 40 minutes for analysis.

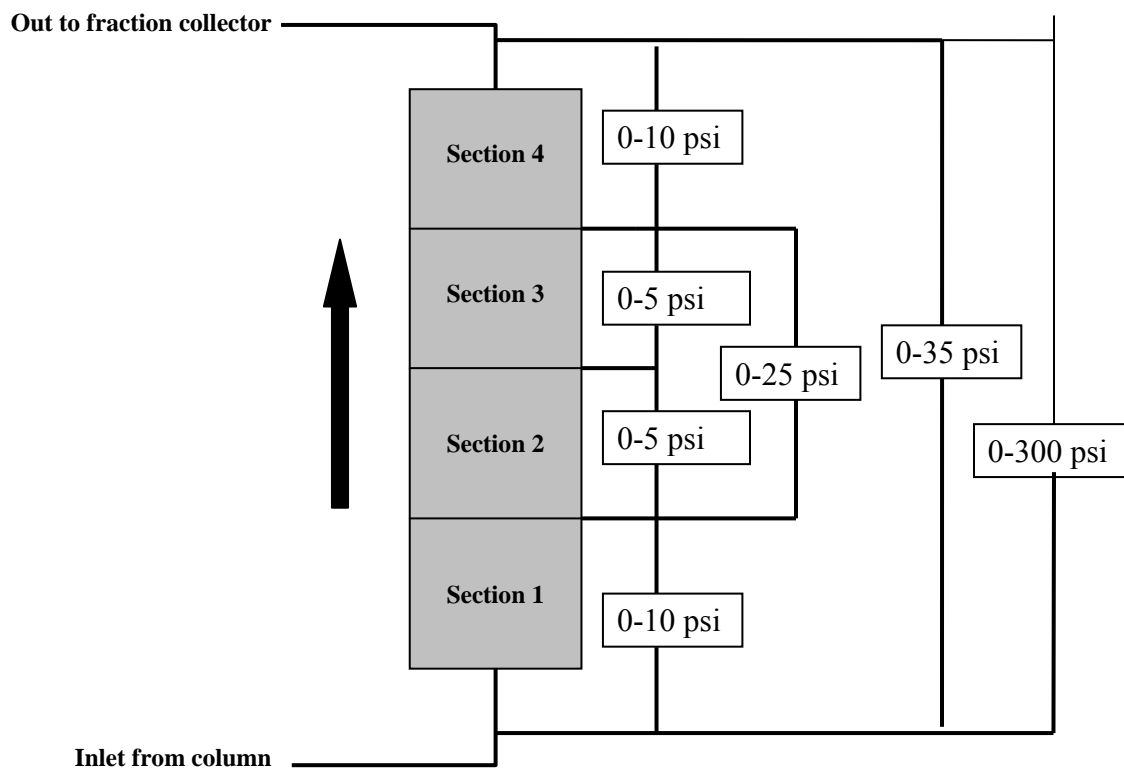
The core was initially saturated with Synthetic Brine (SB) (Table 4.2) and the pore volume of the core was determined by a high salinity tracer test. The core was then flooded with the Crude Oil (Table 4.1) at a constant 100 psi pressure to saturate it with oil. Water flooding, to simulate secondary oil recovery, followed the oil flood to reach and then measure the residual oil saturation in the core. After the water flood, the chemical flood began to replicate tertiary/enhanced oil recovery. The ASP (alkali-surfactant-polymer) slug followed by the polymer drive was injected to the core at 0.1 ml/min. Oil saturations were calculated by material balance during each stage of flooding, and the permeability was calculated using the pressure drop across the core during flooding.

**Table 4.4** Core Properties of Core flood #1

<b>Properties</b>	<b>#1 Core</b>	<b>Units</b>
<b>Mass</b>	1213.06	g
<b>Porosity</b>	0.192	
<b>Length</b>	28.575	cm
<b>Diameter</b>	5.03	cm
<b>Length to Tap 1</b>	5.08	cm
<b>Length to Tap 2</b>	13.97	cm
<b>Length to Tap 3</b>	19.05	cm
<b>Area</b>	20.27	cm <sup>2</sup>
<b>Temperature</b>	85	°C
<b>Air permeability</b>	n/a	md
<b>Brine permeability</b>	234	md
<b>Pore volume (PV)</b>	110	ml

**Table 4.5** Core Properties of Core flood #2

Core	#2 Core	
Mass	1198	g
Porosity	0.201	
Length	28.575	cm
Diagonal	5.03	cm
Length to Tap 1	5.08	cm
Length to Tap 2	14.61	cm
Length to Tap 3	23.5	cm
Area	19.86	cm <sup>2</sup>
Temperature	85	°C
Air permeability	n/a	md
Brine permeability	356	md
PV	114	ml

**Figure 4.3.** #1 and #2 ASP flood set-up.

### 4.3. Results and Discussion

#### 4.3.1. Phase Behavior

The main goal for this phase behavior screening was to find the suitable surfactant formulation with an oil solubilization ratio above 10 for the 50% oil scan (WOR of 1). Guerbet alkoxy sulfate surfactants have previously been studied at the air-water and oil-water interfaces.<sup>28</sup> For chemical EOR, Guerbet alkoxy sulfates have been successfully used in surfactant formulations with temperatures at 85 °C under a wide range of salinity conditions to produce ultra-low interfacial tensions and low microemulsion viscosities. Phase behavior experiments performed with different formulations are tabulated in table 4.3. During the initial phase of screening with crude oil #1 (properties in Table 4.1), much of the selection process was based on qualitative criteria, and many surfactant formulations were ruled out due to the presence of persistent microemulsion (Experiment No. 1,3,8,9, etc.). Initial formulations which contained C-20 carbon chain did not give the required oil solubilization ratio; therefore the aqueous solubility tests were unnecessary. The next available Guerbet alkoxy sulfate was C28-7PO-2EO-Sulfate which was tested with different co-surfactants and co-solvents. Even though high solubilization ratios were obtained in some of the formulations (Ex. No. 12), there was a problem with the aqueous solubility. Therefore, Guerbet alkoxy sulfates with high numbers of ethoxy groups were required to meet the aqueous solubility requirements.

Further studies increasing the carbon number in the Guerbet alkoxy sulfate were more promising when C32-7PO-6EO-Sulfate was considered as a possible candidate.

According to initial phase behavior studies, the Internal Olifin Sulfonates (IOS) were used as secondary surfactants because the microemulsions formed less viscous than the phase

without IOS. In this particular oil, using a C<sub>20-24</sub> IOS with a C32 Guerbet alkoxy sulfate produced favorable results. Therefore, different ratios of C32-7PO-6EO-Sulfate and C<sub>20-24</sub> IOS were studied with different co-solvents TEGBE and MA-80-I in phase behavior experiments. At first 0.5%wt. C32 -7PO-6EO-sulfate, and 0.5%wt. C<sub>20-24</sub> IOS were used in the formulations with 0.5 % TEGBE. Although a microemulsion with a high solubilization ratio (23.3) formed at 3.75-4%wt. sodium carbonate, the desired aqueous solubility was not achieved. Therefore, to obtain a temporally aqueous stability MA 80-I was decided to use with TEGBE as co-solvents.

First 0.5% wt.C32-7PO-6EO-sulfate, 0.5%wt. C<sub>20-24</sub> IOS and 0.5%wt. TEGBE were tested for aqueous solubility test with increasing levels of MA-80-I(MA scan) at 4.5%wt. sodium carbonate to come to the conclusion that 0.4%wt. MA-80-I was sufficient for the aqueous solubility. Next, this formulation with 0.4%MA-80-I was used in a phase behavior experiments where different WOR were studied in addition to the sodium carbonate scans to find the solubilization ratios. The solubilization ratios of 10%, 20%, 30%, 40%, 50% Crude Oil (properties in Table 4.1 ) at 85 °C as a function of sodium carbonate concentration ( presented in Figure 4.4-4.8 )for a formulation consisting of 0.5% C32-7PO-6EO sulfate, 0.5% C<sub>20-24</sub> IOS 0.5% TEGBE,) and 0.4% MA-80-1. The optimum salinities of this formulation are 36,000 ppm, 32,500 ppm, 38,500 ppm, 40,000 ppm and 40,000 ppm respectively. As previously discussed, a solubilization ratio of 10 (or higher corresponds to an interfacial tension of approximately  $10^{-3}$  dyne/cm which is sufficiently low for chemical flooding. The aqueous solubility limit was 45,000 ppm sodium carbonate with 2500 AN 125 polymer and it was clear 45min at 85°C.

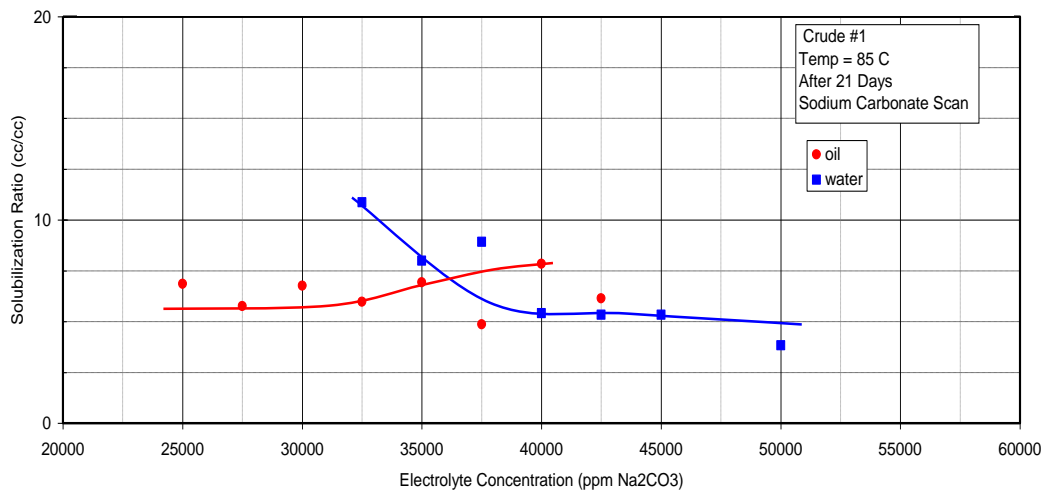


**Figure 4.4.** Solubilization ratio as a function of sodium carbonate concentration for 10% crude oil #1 and the formulations of experiment 23 at 85 °C.

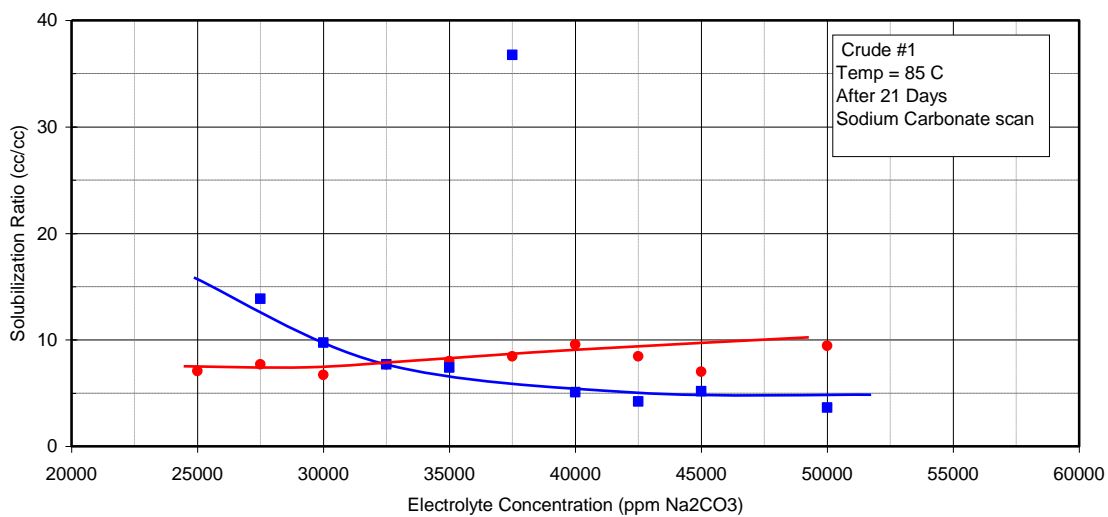


**Figure 4.5.** Solubilization ratio as a function of sodium carbonate concentration for 20% crude oil #1 and the formulations of experiment 23 at 85 °C.

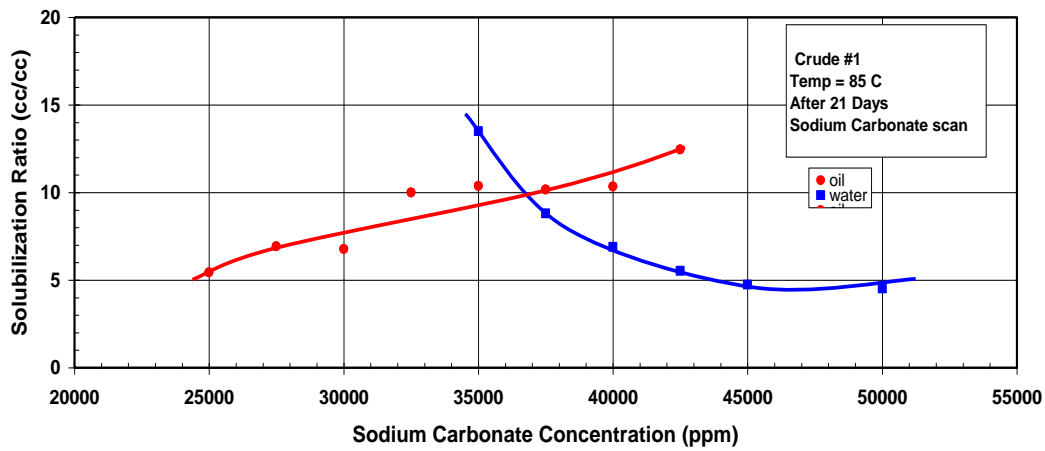


**Figure 4.6.** Solubilization ratio as a function of sodium carbonate concentration for 30% crude oil #1 and the formulations of experiment 23 at 85 °C.

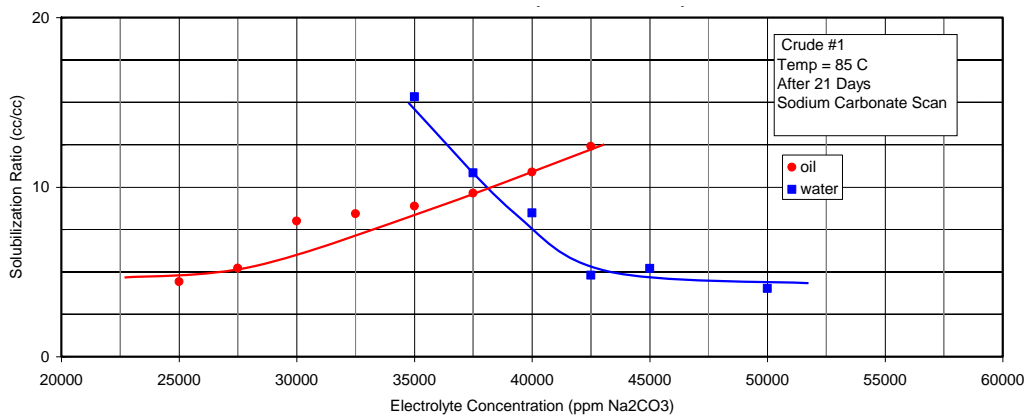


**Figure 4.7.** Solubilization ratio as a function of sodium carbonate concentration for 40% crude oil #1 and the formulations of experiment 23 at 85 °C.

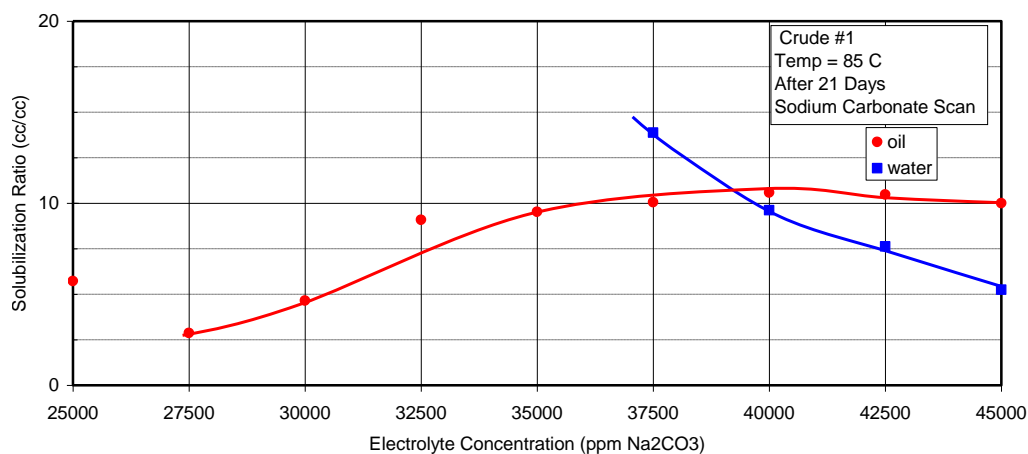


**Figure 4.8.** Solubilization ratio as a function of sodium carbonate concentration for 50% crude oil #1 and the formulations of experiment 23 at 85 °C.

In order to minimize the cost of the surfactants the total concentration of surfactants was reduced by half giving the formulation consisting of 0.25%wt. C32-7PO-6EO sulfate, 0.25%wt. C<sub>20-24</sub> IOS, and 0.25% TEGBE, and 0.4% MA-80-1 (determined by MA 80 scan). Phase behavior experiments showed high solubilization ratios of about 17.5 at the optimum salinity of about 32,500 ppm Na<sub>2</sub>CO<sub>3</sub> with 40% oil (WOR 1.5). The solubilization ratios of the 10%, 20%, 30%, and 40%, Crude Oil #1 phase behavior experiments, as a function of sodium carbonate concentration, are presented in Figures 4.9-4.12 for this formulation. The aqueous solubility limit for this formulation was found at 50,000 ppm sodium carbonate with 2,500 ppm AN 125 polymer and it was clear 45min at 85 °C. Therefore, this formulation (Experiment 24) had a sufficiently low IFT, aqueous solubility at optimum of 3.25%wt. sodium carbonate, and a low-viscous middle phase which leads to the next experimental phase a core flood.

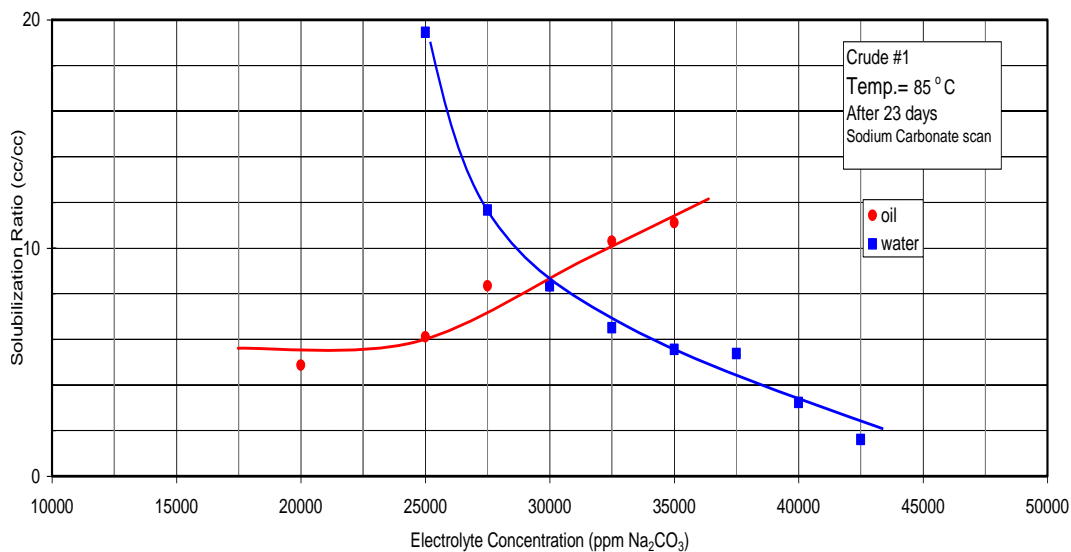


**Figure 4.9.** Solubilization ratio as a function of sodium carbonate concentration for 10% crude oil #1 and the formulations of experiment 24 at 85 °C.  
 EX-24: 0.25% Guerbet C32-7PO-6EO-Sulfate, 0.25% C20-24 IOS, 0.25% TEGBE, 0.4% Aerosol MA-80I in SSB at 85 C (20% Oil)

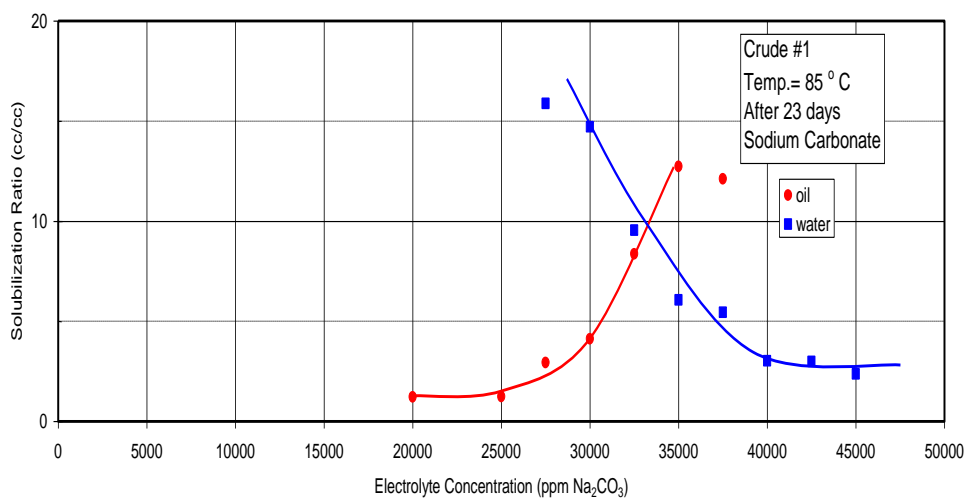


**Figure 4.10.** Solubilization ratio as a function of sodium carbonate concentration for 20% crude oil #1 and the formulations of experiment 24 at 85 °C.

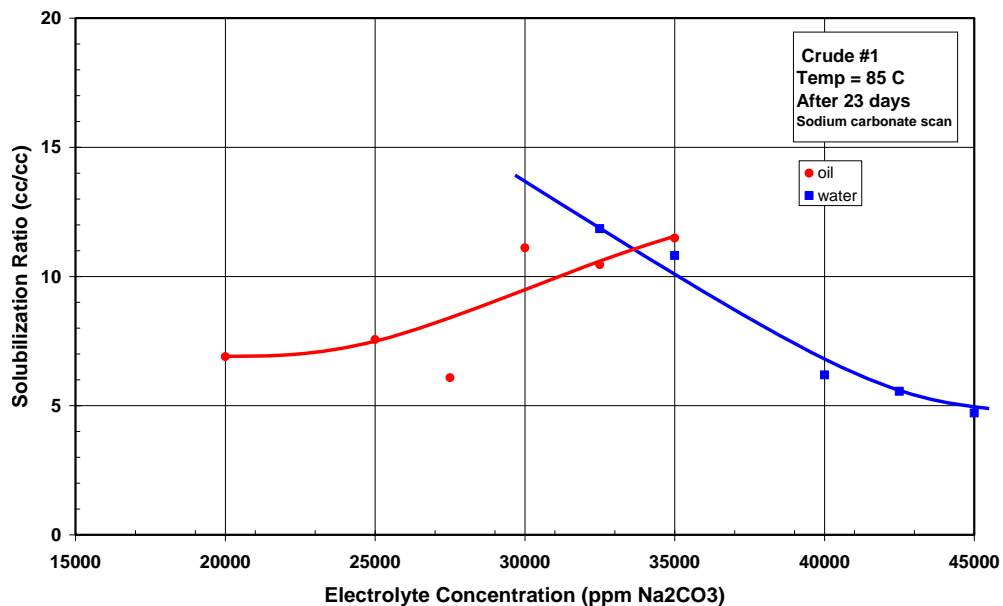


**Figure 4.11.** Solubilization ratio as a function of sodium carbonate concentration for 30% crude oil #1 and the formulations of experiment 24 at 85 °C.

EX-24 0.25% Guerbet C32-7PO-6EO Sulfate, 0.25% C20-24 IOS, 0.25% TEGBE,  
0.4% Aerosol MA-80I in SSB at 85° C (40% Oil)

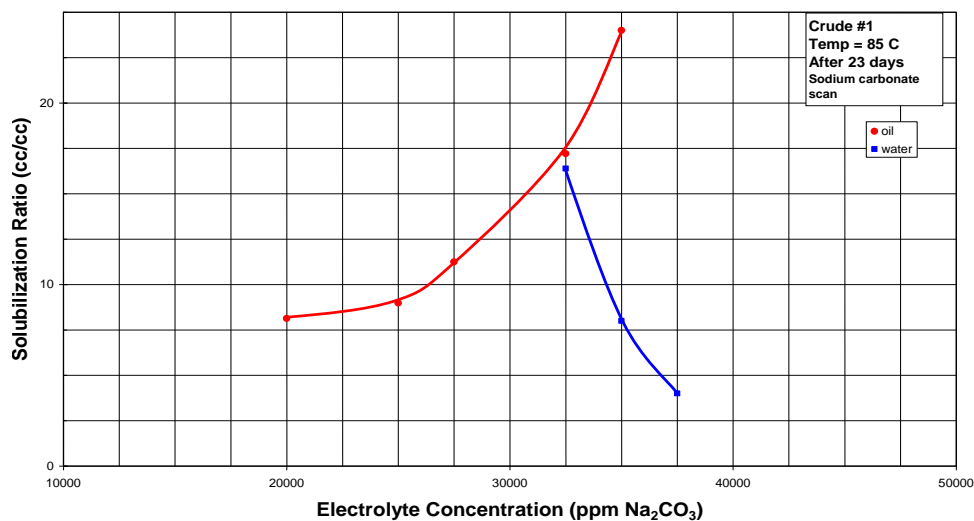
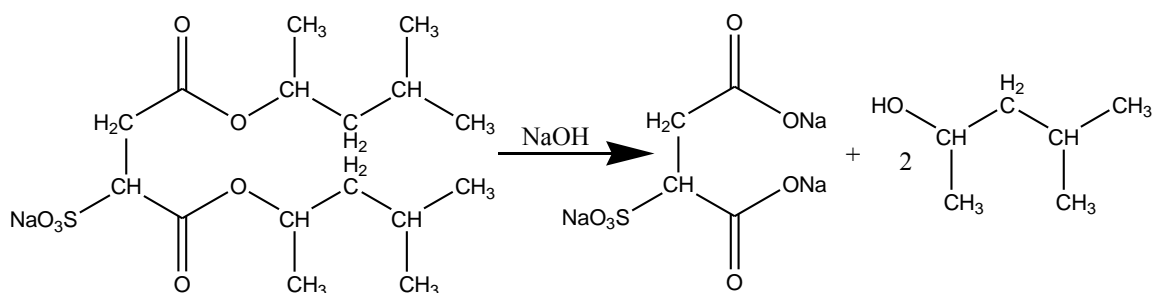


**Figure 4.12.** Solubilization ratio as a function of sodium carbonate concentration for 40% crude oil #1 and the formulations of experiment 24 at 85 °C.

An alternative to co-solvents for improving aqueous solubility for large hydrophobe surfactants is to use a powerful solubilizer such as dihexyl sulfosuccinate (MA 80-I, see Fig 4.13).<sup>27</sup> The MA 80-I is also known as a sacrificial surfactant because it provides aqueous stability temporarily and later hydrolyses in the presence of alkali to 4-methyl-2-pentanol. The hydrolysis reaction occurs faster at elevated temperature and high pH. Unlike traditional co-solvents MA 80-I impacts phase behavior by decreasing optimum salinity because hydrophobic branch pentanol is entered to the surfactant solution after hydrolysis.



MA 80-I

**Figure 4.13.** Hydrolysis of MA 80-I in basic medium.

### 4.3.2. Core floods

Ultimately, Core floods were performed using both the formulations of experiments 23 and 24. Figures 4.14 and 4.15 shows the oil recovery data for both formulations.

Cumulative oil recovery curves show the collection of free oil during the experiments.

The aqueous and oil volumes in the sample tubes were measured immediately after collection. However for increasing accuracy, the volume level was measured after using a centrifuge for about 2 min at 1000 rpm and subsequent re-heating to 85 °C. The total oil

recovery was calculated to be 96.9% of the residual oil in Core flood 1 for the formulation with 0.5% C32-7PO-6EO sulfate, 0.5% C<sub>20-24</sub> IOS and 0.5% TEGBE and 0.4% MA-80-I. The total oil recovery was 97.6% for the formulation with 0.25% C32-7PO-6EO sulfate, 0.25% C<sub>20-24</sub> IOS and 0.25% TEGBE, and 0.4% MA-80-I.

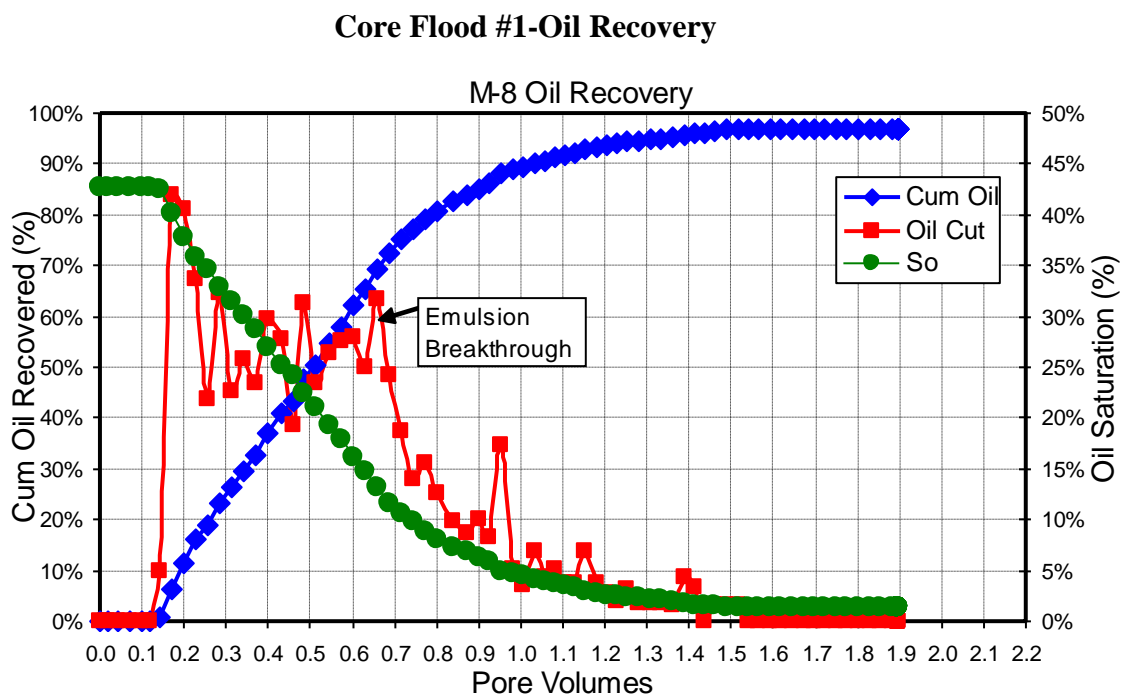


**Figure 4.14.** Oil Recovery data for core flood #1.

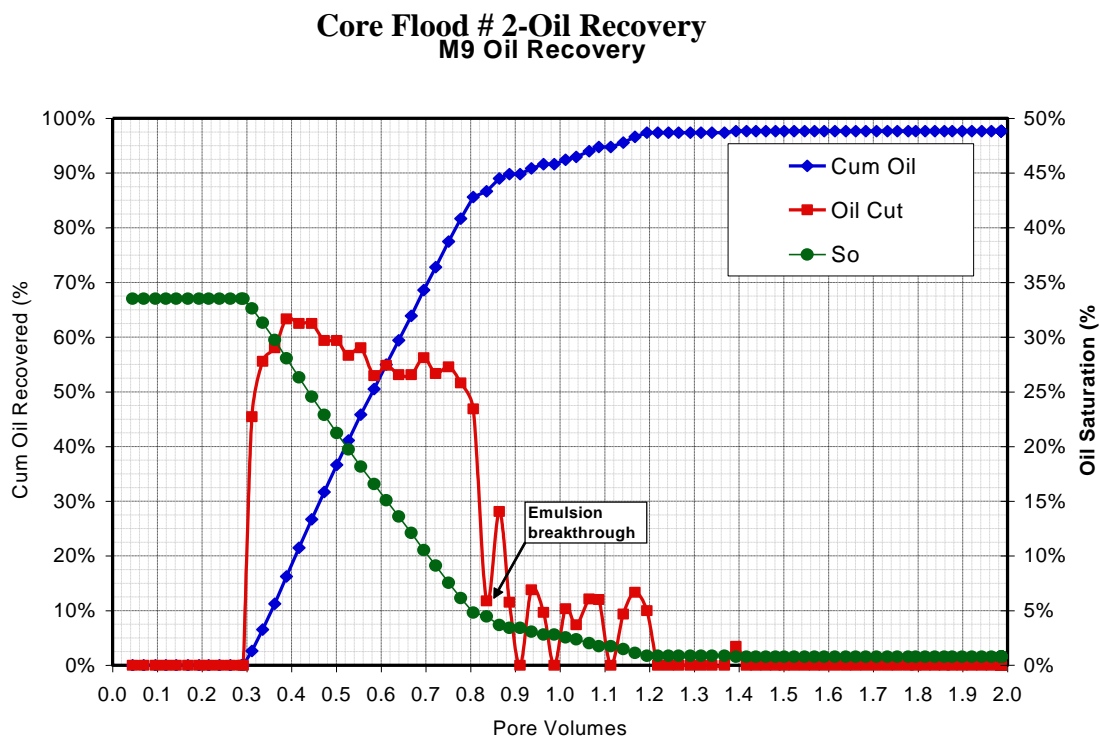


**Figure 4.15.** Oil Recovery data for core flood #2.

#### 4.4. Conclusions

The Guerbet reaction is a very attractive, commercially viable process for producing very large hydrophobe structures. Anionic surfactants are produced by the addition of ethylene oxide and/or propylene oxide to the Guerbet alcohol, followed by sulfation. Sulfation reaction was carried out using sulfamic acid as a sulfation reagent.

Recent advances with novel surfactants and the introduction of Guerbet alkoxy sulfate surfactants as new EOR chemicals have shown an increasingly promising potential for low cost, high efficiency chemical EOR processes. From phase behavior screening and core flood results, Guerbet alkoxy sulfate surfactants have demonstrated their effectiveness. For the target reservoir oil, showing ultra-low interfacial tensions of about  $3 \times 10^{-3}$ , and high oil recovery of 96.9% have been shown for the surfactant formulation

consisting of 0.5% C32-7PO-6EO sulfate, 0.5% C<sub>20-24</sub> IOS and 0.5% TEGBE and 0.4% MA-80-I. Using 0.25% C32-7PO-6EO sulfate, 0.2% C<sub>20-24</sub> IOS and 0.5% TEGBE and 0.4% MA-80-I formulation  $1.3 \times 10^{-3}$  of IFT and 97.6% oil recovery was obtained.

Therefore branched Guerbet alkoxy sulfate surfactants can be categorized as most promising classes of EOR surfactant due to their excellent performance for this reservoir oil. MA-80-I was used to obtain temporally aqueous stability and to prove the concept of sacrificial surfactant.

#### 4.5. References

1. Babadagli, T. *J. Petrol. Sci. Eng.* **2003**, 37,25-37.
2. Steinbrenner, U.; Bittner, C.; Oetter, G.; Guzmann, M. Use of Surfactant Mixture for Tertiary Oil Extraction. U.S. Patent 20090270281A1, Oct. 29, 2009.
3. Taylor, K. C.; Nasr, H.A. *J. Petrol. Sci. Eng.* **1998**,19,265-280.
4. Schumcher, M. M. Enhanced Recovery of Residual and Heavy Oil, Noyes Data Corporation; Park ridge, New Jersey, 1980; Vol. 2, pp.32-64.
5. Groot, M. De. Flooding process For Recovering Oil From Subterranean Oil-Bearing Strata. U. S. Patent 1,823,439, 1929.
6. Gogarty, W. B.; R. W. Olson, US patent Application, filed July 24, 1962.
7. Levitt, D.B.; Jackson, A.C., Heinson, C., Britton, L.N., Malik, T., Dwarakanath, V., Pope, G. A. Identification and Evaluation of High performance EOR Surfactant, SPE 100089, presented at SPE/DOE IOR Symposium, Tulsa, OK, April 2006.
8. Healy, R. N., Reed, R. L. and Stenmark, D. K.: "Multiphase Microemulsion Systems," *SPEJ*, (June 1976), 147-160.
9. Huh, C. *J. Colloid Interf. Sci.* **1979**, 71, 408-426.
10. Winsor, P. A.: *Solvent Properties of Amphiphilic Compounds* Butterworths, London (1954).
11. Gogarty, W. B.; Tosch, W. C. *J. Petrol. Technol.* **1968**, 1407-1414.

12. Austad, T.; Milter, J. Surfactant Flooding in Enhanced Oil Recovery in *Surfactants: Fundamentals and Applications in the Petroleum Industry*, edited by L.L. Schramm, Cambridge University Press (2000), 203-249.
13. Nelson, R. C.; Lawson, J. B.; Thigpen, D. R.; Stegemeier, G. L. Cosurfactant - Enhanced Alkaline Flooding, SPE 12672, presented at the SPE/DOE Fourth Symposium on Improved Oil Recovery in Tulsa, Oklahoma, 15-28 April (1984).
14. Healy, R. N.; Reed, R. L. Physicochemical Aspects of Microemulsion Flooding, *SPEJ*, (October 1974), 491-501.
15. Aoudia, M.; Wade, W. H.; Weerasooriya, V. *J. Dispersion Sci. Technol.* **1995**, *16*,115.
16. Taber, J. J. Research on Enhance Oil Recovery: Past, Present, an Future. Symposium on Surface Phenomenon in Enhanced Oil Recovery. Stockholm, Sweden .August 1975.
17. Lake,L.W.;Enhanced oil recovery/Larry w. Lake. Englewood Cliffs, N. J.; Prentic Hall, c1989,89-95.
18. Salager, J.; Anton, R. E.; Sabatini, D. A.; Harwell, J. H.; Acosta, E. J.; Tolosa, L. I. *J. Surfactants Deterg.* **2005**, *8*, 3.
19. Zhang, D. L., Liu, S., Yan, W., Puerto, M., Hirasaki, J., Miller, C. A., Favorable Attributes Of Alkali-Surfactant-Polymer Flooding, SPE 99744, presented at the SPE/DOE Symposium on Improved Oil Recovery in Tulsa, Oklahoma, 22-26 April (2006).

20. Adkins, S.; Liyanage, P. J.; Pinnawala Arachchilage, G. W. P.; Mudiyansele, T.; Weerasooriya, U.; Pope, G. A. A new process for Manufacturing and Stabilizing High-Performance EOR Surfactants at Low Cost for High-Temperature, High Salinity Oil Reservoirs, SPE 129923 presented at SPE IOR Symposium, Tulsa, OK, 25-28 April 2010.
21. Liu, Q.; Dong, M.; Ma, S.; Tu, Y. *Colloids Surf.* **2007**, *293*, 63.
22. O'Lenick Jr., A. *J. Surfactants Deterg.* **2001**, *4*, 311-315.
23. O'Lenick Jr., A. J.; Parkinson, J. K., *J. Am. Oil Chem. Soc.* **1996**, *73*, 935-937.
24. O'Lenick, Jr.; Anthony, J. Bi-modal Guerbet alkoxy sulfate surfactants. U.S. Patent 7,119,125, Oct. 10, 2006.
25. Flaaten, A.; Nguyen, Q.; Pope, G. A.; Zhang, J. A synthetic Laboratory Approach to Low-cost ,High-performance Chemical Flooding. SPE Improved Oil Recovery Symposium Tulsa, OK, 2008, 19-23.
26. Tally, L.D, Hydrolytic Stability of Alkylethoxy Sulfates. *SPE Reservoir Engineering*, *3*(1), 1988, 235-242.
27. Varadaraj, R.; Bock, J.; Valint, P., Jr.; Zushma, S.; Thomas, R. *J. Phys. Chem.* **1991**, *95*, 1671-6.
28. Yang, H.; Britton, C.; Liyanage, P. J.; Solairaj, S.; Kim, D. H.; Nguyen, Q.; Weerasooriya, U.; Pope, G. A. SPE 129978 presented at SPE IOR Symposium, Tulsa, OK, 25-28 April, 2010.

## Appendix

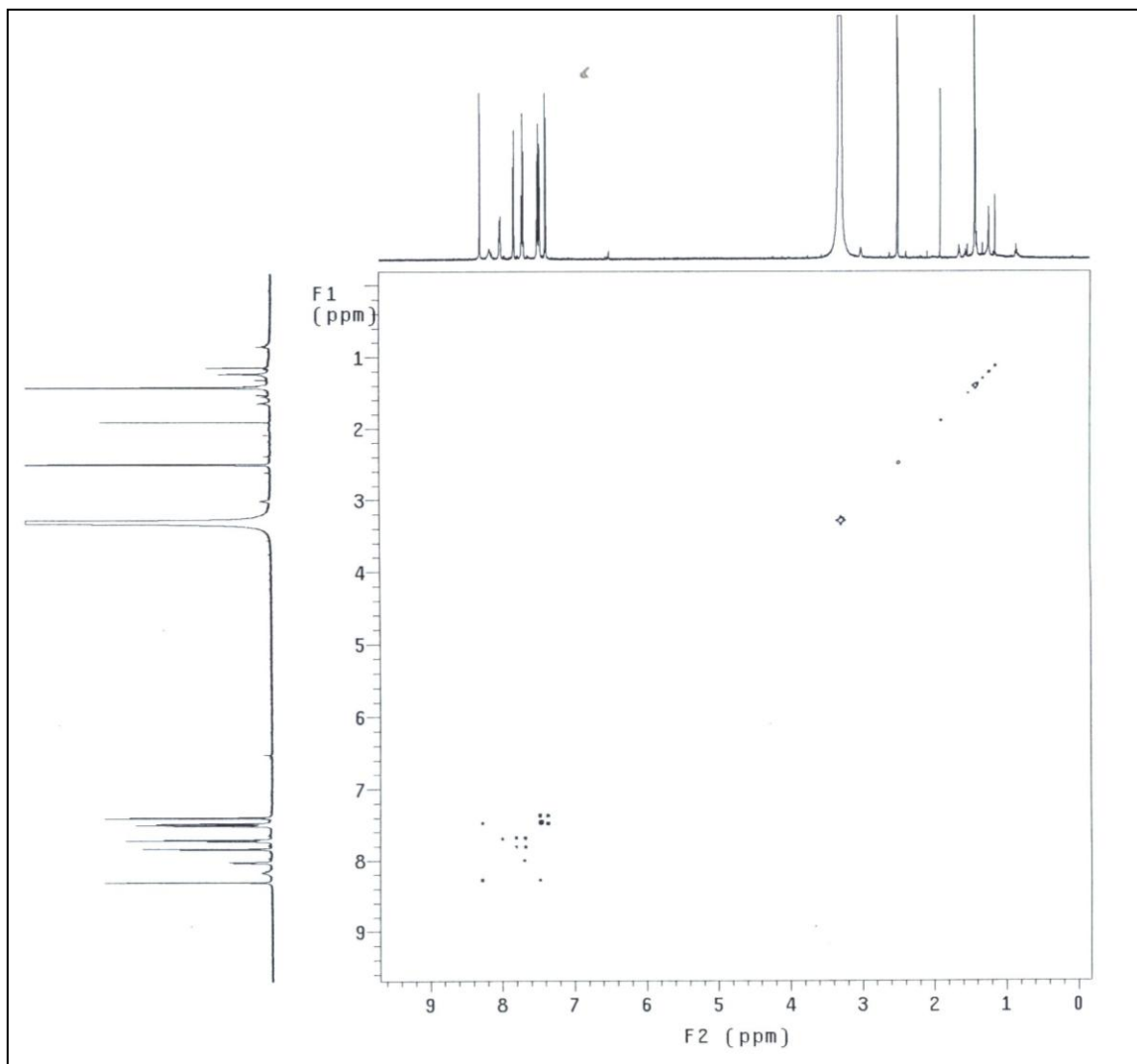


**Figure A1.** HSQC spectrum of 2-cyano-3-(4-(2-(5-(2-(4-(3,6-di-*tert*-butyl-9*H*-carbazolyl)phenyl)ethynyl)-2,2'-bithiophenyl)ethynyl)phenyl)acrylic acid (**1**) in DMSO (600MHz) .

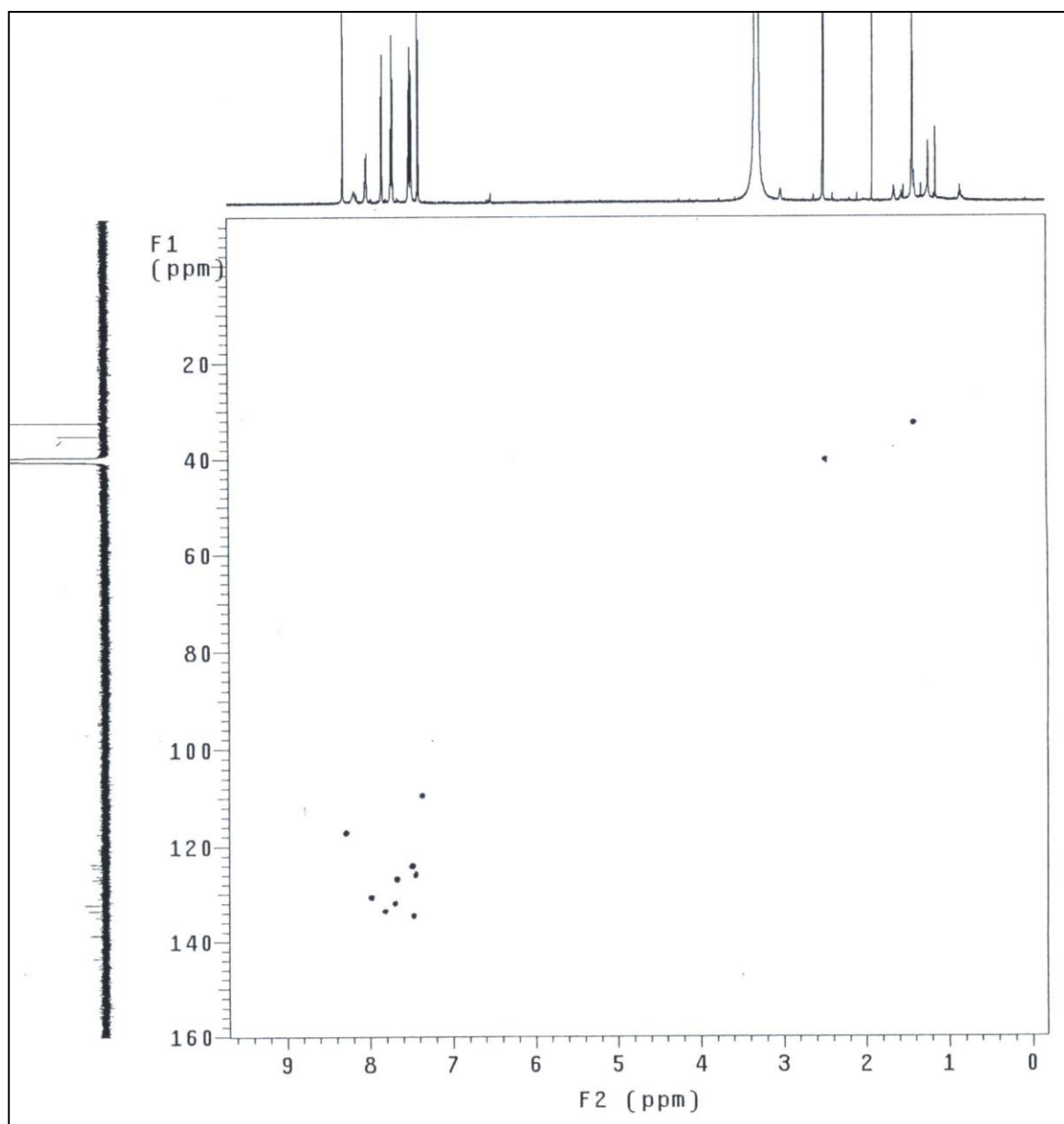


**Figure A2.** HSQC spectrum of 2-cyano-3-(4-(2-(5-(2-(4-(3,6-di-*tert*-butyl-9*H*-carbazolyl)phenyl)ethynyl)-2,2'-bithiophenyl)ethynyl)phenyl)acrylic acid (**1**) in DMSO (600MHz) .

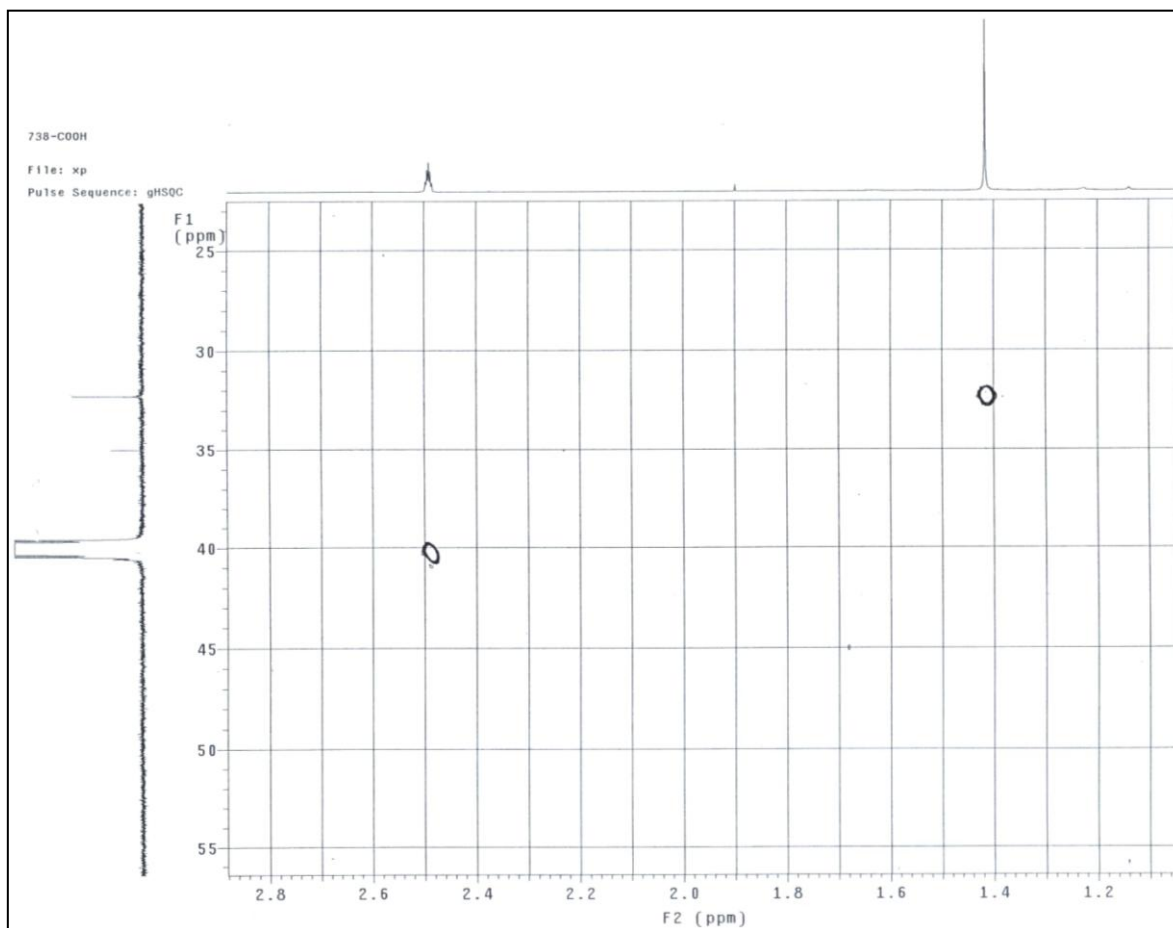


**Figure A3.** HSQC spectrum of 2-cyano-3-(4-(2-(5-(2-(4-(3,6-di-*tert*-butyl-9*H*-carbazolyl)phenyl)ethynyl)-2,2'-bithiophenyl)ethynyl)phenyl)acrylic acid (**1**) in DMSO (600MHz) .

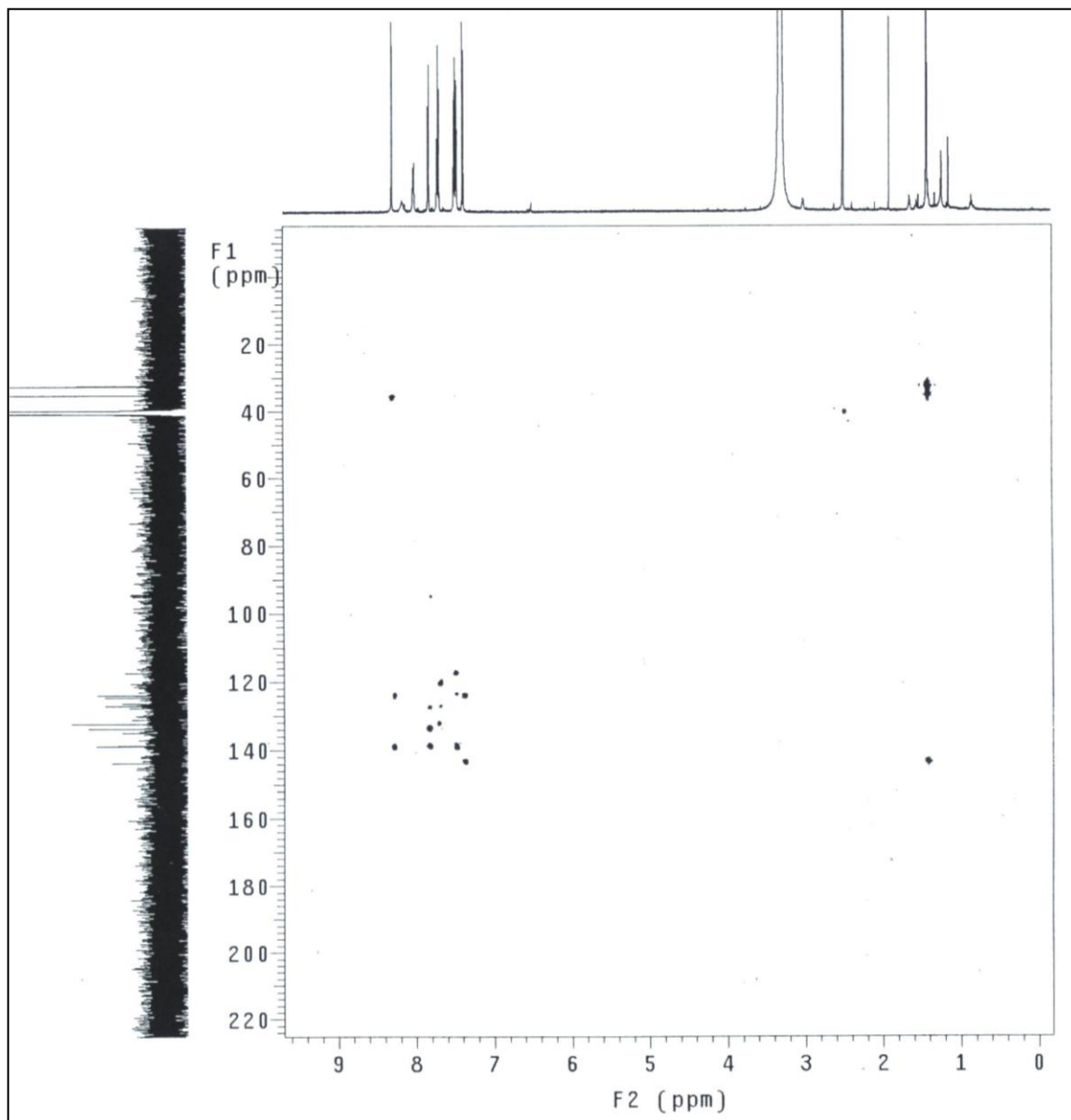


**Figure A4.** HMBC spectrum of 2-cyano-3-(4-(2-(5-(2-(4-(3,6-di-*tert*-butyl-9*H*-carbazolyl)phenyl)ethynyl)-2,2'-bithiophenyl)ethynyl)phenyl)acrylic acid (**1**) in DMSO (600MHz) .

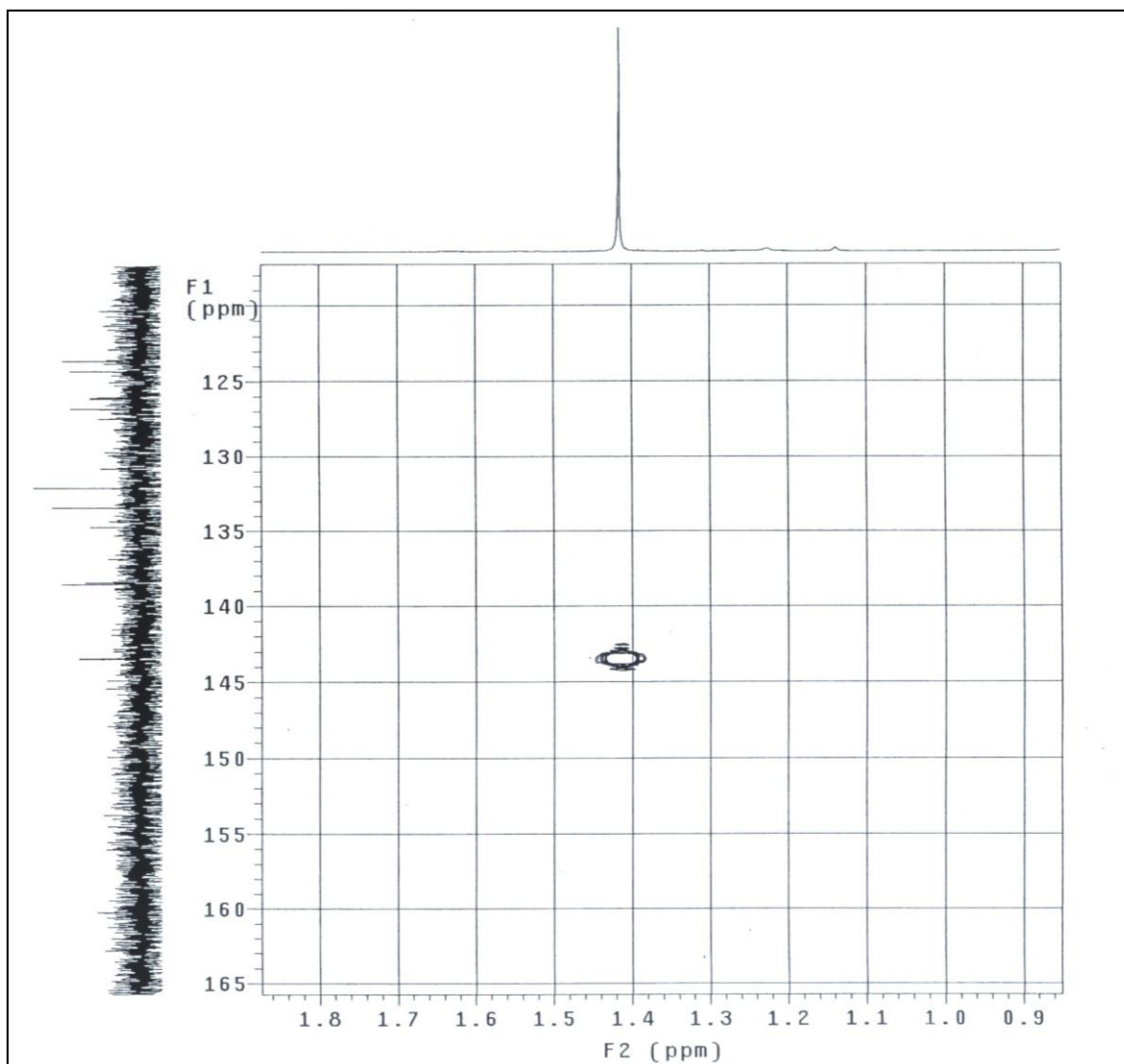


**Figure A5.** HMBC spectrum of 2-cyano-3-(4-(2-(5-(2-(4-(3,6-di-*tert*-butyl-9*H*-carbazolyl)phenyl)ethynyl)-2,2'-bithiophenyl)ethynyl)phenyl)acrylic acid (**1**) in DMSO (600MHz) .

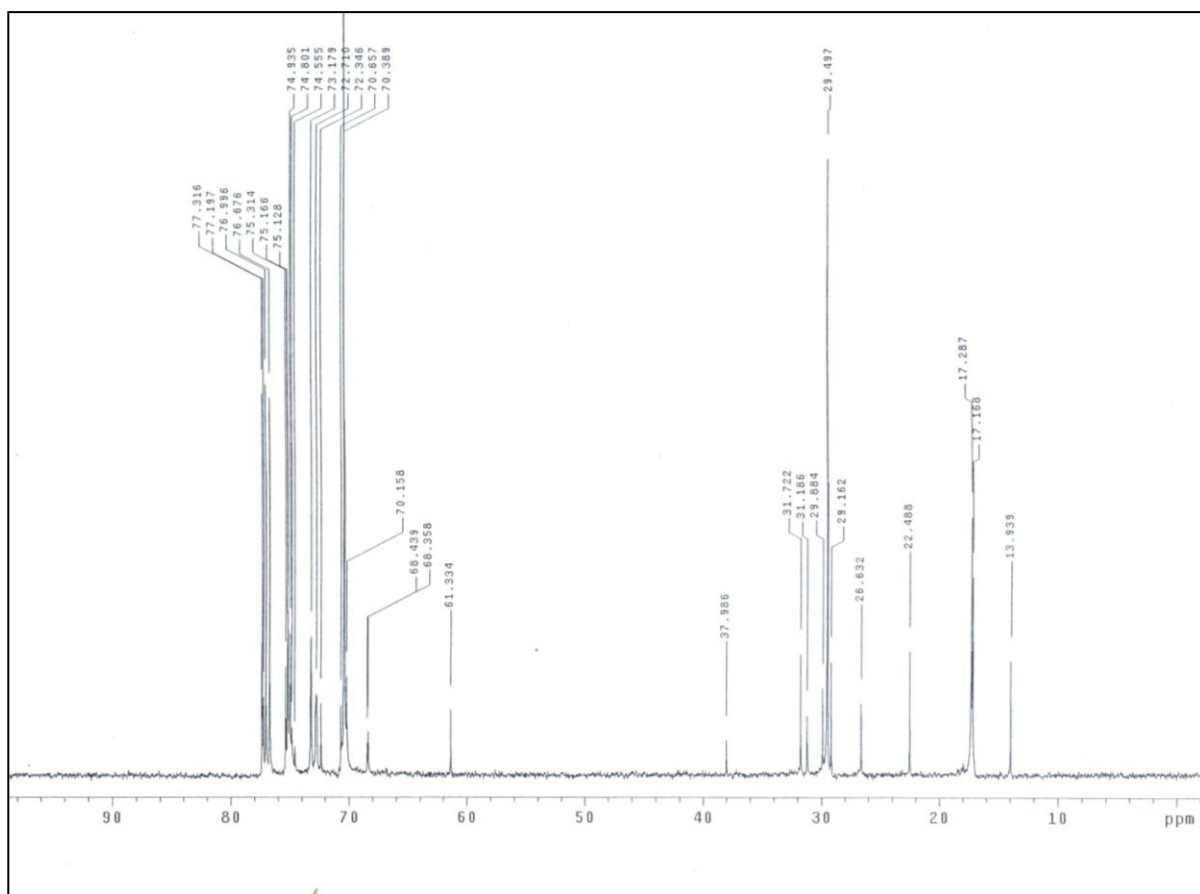


**Figure A6.**  $^{13}\text{C}$  NMR spectrum of Gurrbet  $\text{C}_{32}\text{H}_{65}\text{-7PO-6EO-OH}$ .

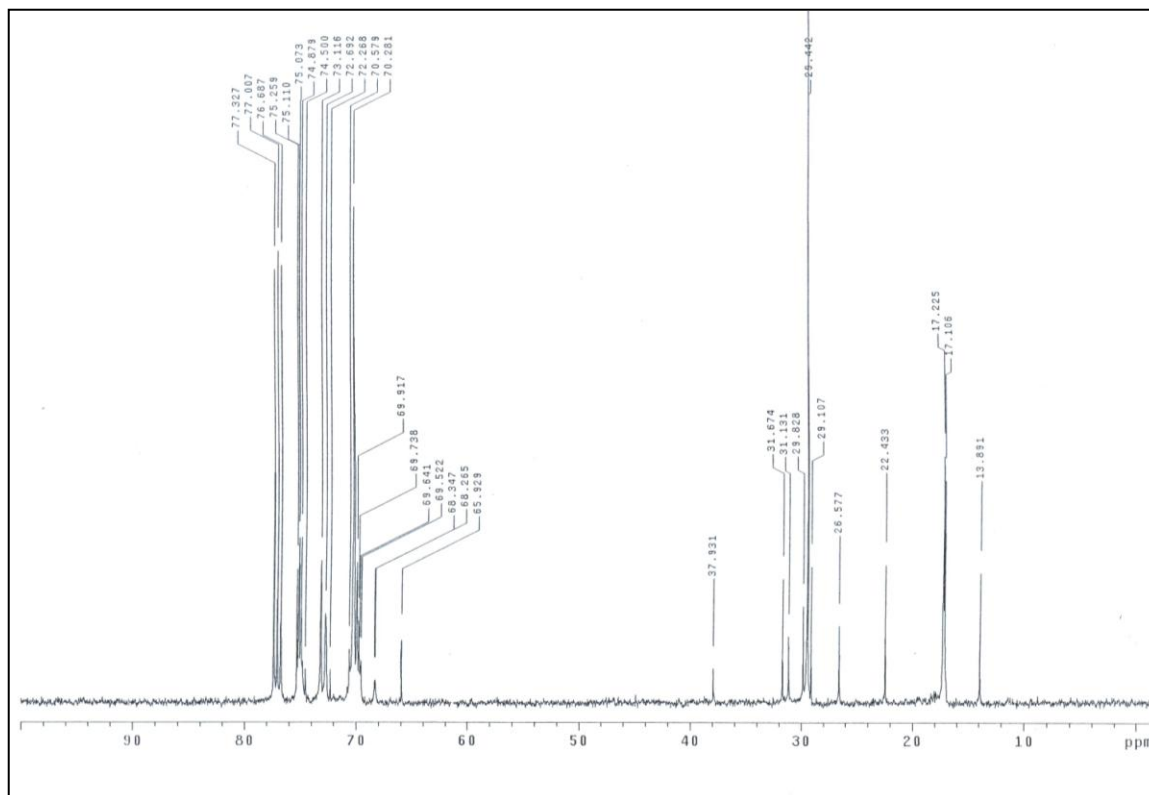


**Figure A7.**  $^{13}\text{C}$  NMR spectrum of Gurrbet  $\text{C}_{32}\text{H}_{65}\text{-7PO-6EO-sulfate}$ .